Biomass and Bioenergy 201 (2025) 108037

Contents lists available at ScienceDirect

Biomass and Bioenergy

journal homepage: www.elsevier.com/locate/biombioe

Performance enhancement of SI engine through LIVC miller cycle approach with Producer gas-biogas blends: A simulation and optimization study

Lawalesh Kumar Prajapati, Jeewan Vachan Tirkey *

Department of Mechanical Engineering, Indian Institute of Technology (BHU), Varanasi, 221005, India

ARTICLE INFO

Keywords:
Producer gas and biogas
Late inlet valve closing
RSM
Engine performance
Exhaust emission

ABSTRACT

There are many difficulties by using a sole renewable energy source. In this view, the current research intends to use producer gas (PG) and biogas (BG) blend in equal volume produced by waste biomass via gasification and anaerobic digestion. The purpose of this research is to enhance the performance and reduce the emissions of the SI engine. So, a comprehensive quasi-dimension thermodynamical model has been used to simulate the performance of SI engines with various input variables, such as late inlet valve closure timing (LIVC), start of ignition timing (SOI), and inlet pressure. This work is novel in using FORTRAN code to simulate the impact of LIVC, SOI, and inlet pressure on SI engine performance and emissions. Additionally, It seeks to ascertain the optimum operating parameters for the mordost responsive power, efficiency, fuel usage, and pollution limits. The response-surface methodology was used to optimize the operating and response parameters. Using an ANOVA-based regression model shows 95 % confidence level of accuracy. The optimum operating settings were found 60° aBDC-LIVC, 22.38° bTDC-SOI, and 2.5 bar intake pressure. Corresponding to these optimal inputs, the optimum response performance were found to be 5.10 kW, 28.78 %, 13.30 MJ/kWh, 0.439 (vol%), 1125.9 ppm for indicated power (IP), indicated thermal efficiency (ITE), brake specific energy consumption (BSEC), CO, and NO respectively, with a composite desirability of 0.841. According to the study's findings, modeling and optimization can be used to estimate the overall performance of SI engines that run on a blend of BG and PG fuel.

Nomenclature:

P	Pressure
V	Volume
Q	Heat rate
θ	Crank angle
T_m	Gas mixture temperature
V_c	Clearnce volume
L	Length of connecting rod
CR	Compression ratio
T_w	Cylinder wall temperature
α	Crank angle for two zone combustion
ρ_u	Density
A_f	Flame front area
u_T	Flame velocity
RE	Reynold Number
SOI	Strat of Ignition timing
LIVC	Late Inlet Valve closing

1. Introduction

Today's major issues and challenges are the conventional energy crises versus rising demand and emission reductions required to keep global regular temperature rise well below 2^0C [1]. Electricity is a significant factor in sustainable socio-economic development in developing countries. Currently, around 38 % of the world's prime energy is used to generate power from coal, and at this rate, coal support will continue for the next 137 years [2,3]. On the other side, there is still a global death of electricity, as over 850 million people still do not have regular access to electricity IEA-2019 (International Energy Agency-2019) [4,5]. Furthermore, electric vehicles will significantly raise the need for electricity in the future. It is predicted that the global electric vehicle fleet will reach about 230 million vehicles in 2030 (International Energy Agency (IEA), 2021) [6,7]. Concerning these challenges, it could be concluded that there is no option other than adopting alternate energy resources. Furthermore, a single alternative energy source is difficult to meet energy demand since it has a low energy density, is affected by seasonal variability, and has inconsistent availability, resulting in

* Corresponding author.
E-mail address: jvtirkey.mec@iitbhu.ac.in (J.V. Tirkey).

https://doi.org/10.1016/j.biombioe.2025.108037
Received 12 November 2024; Received in revised form 6 May 2025; Accepted 28 May 2025
Available online 9 June 2025
0961-9534/© 2025 Elsevier Ltd. All rights are reserved, including those for text and data mining, AI training, and similar technologies.

sporadic power supply [8–10]. Therefore, the motivation of this study is to emphasise the use of PG-BG fuel blend in order to conserve conventional fuel and increase efficiency by utilising improved technologies and optimal operating conditions.

In light of the facts mentioned earlier about the energy crisis and environmental safety, biogas is one possible substitute gaseous fuel that could generate electricity and slow down global warming. Because it has the potential to minimize fossil fuel consumption, and its methane component provides emission reductions [11]. Biogas is produced through anaerobiotic absorption, and biological materials (anaerobic organisms) undergo metabolic degradation under specific conditions at temperatures ranging from 25 °C to 350 °C [12,13]. It was reported that an average of approximately one tonne of residue can produce 310 m^3 of biogas [14]. The typical composition of biogas through anaerobic digestion lies in the volumetric percentage of CH_4 (53–70), CO_2 (30–47), H_2O (5–10), H_2S (0-10ppm_v), N_2 (0.3–3 vol%) and various slight impurities including hydrogen sulfide [15,16]. The calorific value of biogas depends on the fraction of methane and CO_2, which is typically found to have a lower calorific value equal to 17 MJ/kg [17,18]. Bharathiraja et al. [19] found that the BG contains a calorific value of 23.1 MJ/m^3. However, the production and composition of biogas are largely influenced by the anaerobic digestion process [20,21]. For instance, Deepanraj et al. [22] conducted anaerobic digestion of food waste and found the optimum operating condition for high yield as solid concentration of 7.5 % TS, pH above 6, 50^{0}C working temperature, and 20.2 C/N ratio. So far as disadvantages is anxious in biogas production, anaerobic digestion is a slow process requiring a long hydraulic retention time (HRT) of >30 days, and this increases the volume of digester and thus respective cost [23]. One of the key challenges in biogas production is the strict requirement for maintaining an optimal operating temperature around 37 °C to ensure stable anaerobic digestion. Deviations from this temperature can severely impact microbial activity, leading to a considerable reduction in biogas yield. Therefore, a reliable and energy-efficient heating system is essential to mitigate the effects of seasonal and diurnal temperature variations throughout the year [23], Furthermore, it has been reported that even a modest rise in temperature from 35 °C to 38 °C can increase microbial mortality, resulting in a noticeable decline in biogas production [24]. In parallel, feedstock variability poses another major constraint. India generates approximately 356.7 million tonnes (Mt) of surplus agricultural biomass annually, with the potential to produce 53,767 MWe of electricity [25]. However, not all biomass is equally suitable for anaerobic digestion. While some residues are readily biodegradable, others are hard or non-biodegradable. To ensure maximum conversion efficiency, a feedstock segregation approach is necessary. Readily biodegradable materials are ideal for biogas production, whereas more recalcitrant biomass types are better suited for alternative processes such as thermal pyrolysis or gasification [26].

In light of the pros and cons of biogas and its limitations, there is another alternative gaseous fuel known as producer gas (PG) or syngas, which is produced by a thermochemical process in the gasifier unit using waste biomass and carbonaceous material as feedstock. In the waste-to-fuel conversion, PG generation through gasification has been known as a potential conversion technique due to its specific advantages such as flexibility in the feedstock, utilization of whole biomass, faster kinetics and improved efficiency [27–29]. The PG has a typical volumetric composition of air gasification: 3–6 MJ/N·m^3 is the lower heating value (LHV) for the mixture, which is composed of 10 % H_2, 12 % CO, 17 % CO_2, 4 % CH_4, and 57 % N_2 [30]. The formation of this composition, especially the production of H_2 and its calorific value, is significantly influenced by the physical and chemical properties of the feedstock, the gasification process as a whole, the gasification agents (such as air, steam, CO_2, oxygen, and their combinations), and the operating temperature [31]. Gasification often occurs in stages, such as drying (0–250 °C), pyrolysis (250–550 °C), oxidation (800–1000 °C), and reduction (800–600 °C)) [32,33]. Regarding the effect of gasification agents, Prando et al. [30] reviewed and compared the air gasification with oxygen, steam, CO_2 based gasification offers enhanced LHV of 10–15, 12–20, 7–10 MJ/N m^3, respectively.

Table 1
Relative thermophysical properties of the associated fuel.

Properties	PG [52]	BG [47]
Composition	Olive biomass [61] H_2: 17-20 CO: 18-21 CH_4: 1-3 CO_2: 8-12 N_2: 45-50	Range (V%) [19] CH_4: 40–75 % CO_2: 15–60 % H_2O: 1–5 % N_2: 0–5 %
Lower heating value (MJ/Nm^3)	3.5–6	17 (MJ/kg)
Density at 1 atm and 15 °C (kg/m^3)	1.05	1.2
Flame velocity at NTP (cm/s)	20–30	25
A/F ratio (kg of air/kg of fuel)	1.2	5.8
Flammability limit (vol% in air) (lean-Rich)	7–21.6	7.5–14
Octane number (RON)	100–105	130
Auto ignition temperature (^{0}C)	625	650
Adiabatic flame temperature at NTP (K)	1800 [62]	~1973 [63]
Minimal initiation energy (MJ)	0.31 [64]	0.465 [45]

Further, in view of decentralised and continuous electric power generation using biogas or producer gas fuel or their blend, one viable technique is using IC engines with genset integration. However, while using PG as the sole fuel for the IC engine, it produces lower brake power (BP) because of PG's low energy density content and volumetric efficiency [34]. Several work has been reported about derating of power as: 45 % power reduction and 18 % overall efficiency in SI engine with sole PG at CR 8.5 [35]; 10 % power derating while PG/Propane blend (55:45) used at 10 CR in SI engine [36]; 19 % power loss with turbocharged SI engine [37]; 12.4 % reduction of power at 12 CR and overall efficiency found to be 21 % at 85 % load [38]; 19 % power reduction with sole PG in SI engine at 14 CR [39]; 20 % derated of SI engine at 11CR and 1 % reduction of brake thermal efficiency (as 27 % of PG and 28 % petrol) [40]. This review shows that SI engines with PG applications can significantly improve by blending higher CV fuel, raising the compression ratio within the knock limit (it has an excellent antiknock tendency), and supercharging fuel intake. In contrast, the benefit of using PG in engines is that significant emissions are reduced. Shah et al. [41] reported that syngas-fueled SI engines can lower CO and NOx emissions by 30–96 % and 54–84 %, respectively, when compared to gasoline, however CO_2 emissions increased by more than 33 %. Indrawan et al. [42] found that a sole Switchgrass-PG-fueled SI engine significantly reduces the CO, NOx, SO_2, and HC emissions across the whole load range, although CO_2 emissions increased noticeably (but decreased with higher load) when compared to natural gas-fueled SI engines. Szwaja et al. [43] investigated a 40 % methane blend in syngas that provides a reasonable engine run in terms of power, but it has no noticeable effect on the reduction of emissions when compared to a pure methane run. Thangaiyan et al. [44] experimental observations showed that utilising syngas and petrol as a dual fuel reduced CO and NO emissions by 22 % and 19 %, correspondingly, as compared to a neat petrol run. Based on the above review, it can be inferred that producer gas possesses a lower calorific value compared to conventional fuels, which directly contributes to reduced engine performance, including lower brake power and overall output.

To overcome the limitations associated with the low calorific value of producer gas, it is beneficial to blend it with biogas, which possesses a relatively higher calorific value. This complementary blending strategy not only enhances the fuel mixture's overall energy content but also leverages each gas's distinct combustion characteristics. While biogas improves the energy density and combustion stability, producer gas contributes with its superior antiknock properties due to its high hydrogen and carbon monoxide content. The synergistic effect of this blend can lead to improved engine performance and reduced knocking

Table 2
Effects of various response settings on the performance and emissions of SI engines.[65–74,86]

Setting	Ranges	BP	BSFC	BTE	CO	NO	Ref.
CR	9-15	↑	↓	↑	↑↓	↑	[17, 52, 53, 65, 66]
ER	0.64-1.5	↑↓	↑↓	↑↓	↓	↑↓	[17, 52, 65, 66]
SOI	8-40 °CA bTDC	↑↓	↓↑	↑↓	↑	↑	[17, 67-69]
Blend on Gasoline	0-80%	↓	↑	↑↓	↑	↑	[17, 66, 68-70]
IVC	10-110°CA-aBDC	↓	↑	↑	↑↓	↑↓	[71, 72]
Speed	1200-3000 rpm	↓	↑	↑	↓	↑	[17, 65, 68]
Intake boost Pressure	0.8-1.6 bar	↑	↓	↑	↑	↑	[73],[74]
Current study							
SOI timing + Intake boost pressure + LIVC timing	30-15° bTDC	↑	↑	↑	↓	↓	Not yet
	1-2.5 bar	↑	↓	↑	Not change	Not change	
	60-85° aBDC	Not change	↓	↑	Not change	Not change	

tendencies under varying inlet pressure conditions. Table 1 shows the detailed comparative thermophysical properties of the fuels. An engine's air intake line can easily induce biogas (bio-methane) via a carburetor or gas flow adjuster, where the gasoline carburetor throttle can control the blended fuel quantity [45]. The application of biogas is more appropriate for SI engine than CI engine, although it can be used in CI engines with blended dual fuel modes [46]. Because biogas has a very high octane number (130 ON, Table .1), it is possible to use a gasoline engine directly with minimal modifications and higher CR to improve thermal efficiency without knocking [47,48]. Also, it has high self-ignition temperate (6500C) in compared to LPG, Natural gas, Hydrogen and PG, which promotes the antiknock feature of the engine [49]. The main composition of biogas is CH_4 and CO_2, and both play significant roles in combustion characteristics. The rise of CH_4 in composition increases the CV of fuel to improve power. Kwon et al. [15] experimentally observed that as CO_2 content increases with CH_4 brake power increases correspondingly. But, the presence of CO_2 lowers the NOx emission due to temperature reduction (because due to its high specific heat CO_2 acts as a heat sink). Consequently, it improves the fuel's anti-knock quality, which further offers to use high CR in engine [9,50]. Regarding engine power and emission characteristics while using biogas in SI engine, the sole biogas produces low power because of its low energy density [17, 47]. Still, it reduces emissions, especially CO and NOx. Experimental research by Hotta et al. [51] revealed that compared to a gasoline-fueled engine, a sole biogas-SI engine has a BP decrease of 17.5 %, CO emission reduction of 39.4 % and NOx emission reduced by 81.5 % at fully opened throttle.

Regarding enhanced power, a raise of compression ratio (CR) in engine is found to be a feasible technique to improve the power and efficiency. Porpatham et al. [52] experimented on a biogas-SI engine, and suggested that while CR rises from 9.3 to 15, the BP improves by 10 % and BTE enhances from 23 % to 26.8 % at 0.94 equivalence ratio but there is marginal decrement of CO level. Similarly, in another study, it was found that spark timing and CR increment significantly change the emission level, while varying CR from 10 to 14, BP increases up to 12 CR then decreases marginally, HC increases simultaneously but CO and NOx decrease substantially after 12 CR with speed (1400–1700 rpm) as well [18]. Successively, regarding performance improvement of the biogas-SI engine, it was suggested that optimization of operating settings (viz. spark timing, CR, equivalence ratio, valve closing, inlet charge condition etc.) and blending with suitable fuel could improve the performance of SI engine [9,53]. So far inlet charge pressure increment is concerned, it promotes knocking of an SI engine. To overcome this, Techniques based on Miller cycles can be used to lessen knock propensity in SI engines and improve engine efficiency. The Miller cycle operation can be achieved through the EIVC or LIVC by adjusting the poppet valve of an engine [54, 55]. Literature [56,57] reports that hybrid electric vehicles prefer Atkinson-based engines because they perform well under limited load conditions [58]. Recent investigations [59,60] have demonstrated that integrating variable intake valve timing (VVT) strategies with turbocharging in SI engines can significantly enhance performance metrics. Turbocharging effectively increases the intake charge density, thereby improving power output; however, it concurrently raises the propensity for knock due to elevated in-cylinder pressures and temperatures. This challenge can be mitigated by implementing the LIVC strategy, which reduces the effective compression ratio and thus suppresses knock formation. Furthermore, the use of variable Miller cycle approaches specifically both LIVC and EIVC in conjunction with Exhaust Gas Recirculation (EGR) has been shown to improve BTE and reduce NO emissions. These synergistic strategies offer a thermodynamically favorable solution for enhancing the efficiency and combustion stability of SI engines, particularly when operating on low-calorific or alternative gaseous fuels such as PG and BG. Table 2 shows the impact of parametric operational factors such as CR, ER, LIVC, SOI, and inlet pressure highly

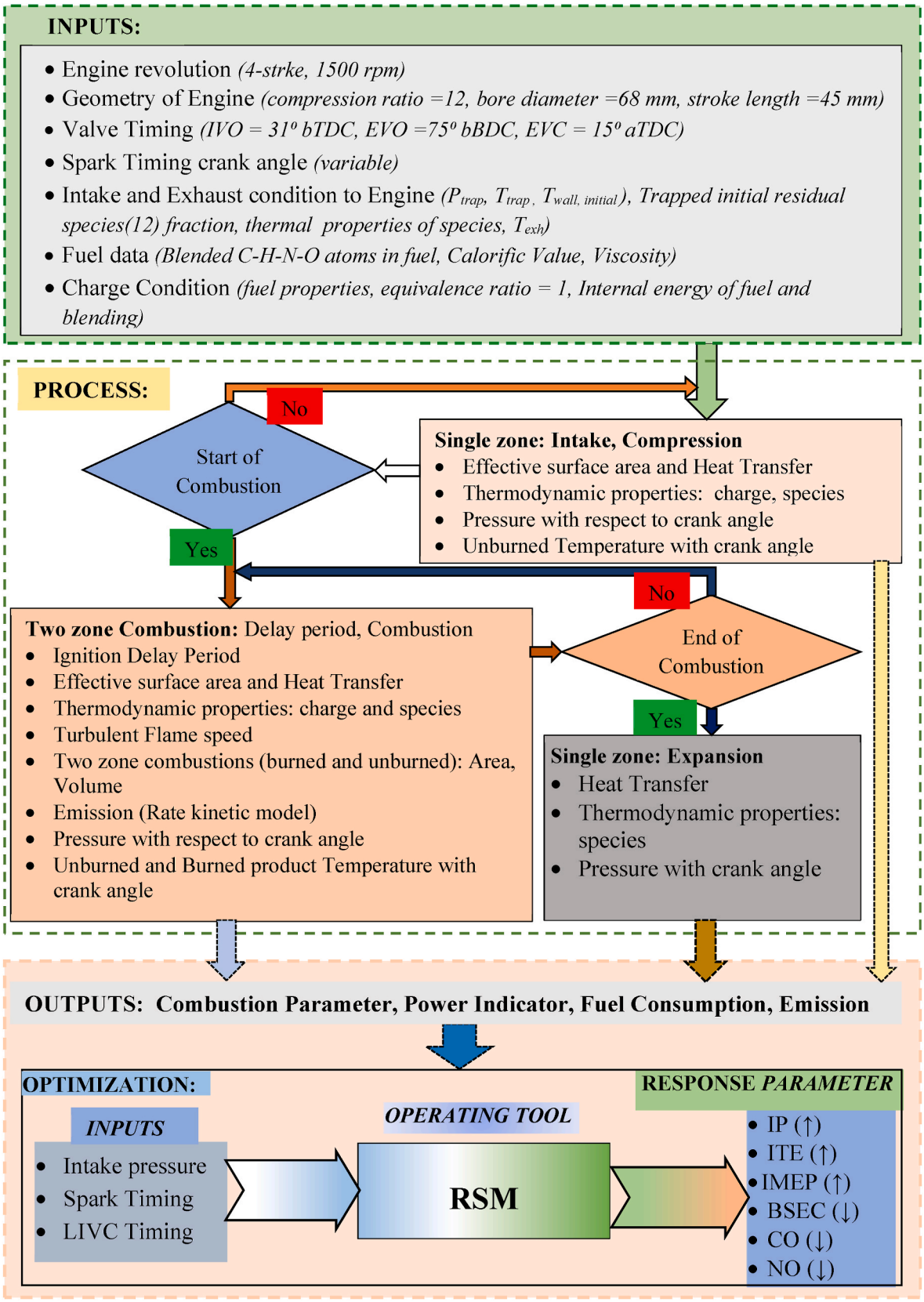

Fig. 1. Thermodynamic simulation and optimization approach.

influences the performance and emissions of SI engines. Different writers have observed trade-offs in the performance of an engine with the variation of these parameters (up or down), but it also depends on fuels and engine configuration. Therefore, while new alternative fuels and their mixing are being investigated for SI engines, the operating settings must be optimized to maximize performance and minimize emissions.

1.1. Motivation and novelty

According to the works mentioned above, the first driving force for this work is to motivate the use of twin energy resources, PG from gasification and BG from anaerobic or landfill digesters, to ensure sustainable alternative energy sources. The second motivation is to establish the viability of PG and BG utilization in SI engines in terms of performance investigation. The third is to determine how to improve the brake power despite the fact that both (PG & BG) have low energy density as compared to gasoline and methane fuel, and then optimize the operational parameter settings for the optimal power and emission (in reference to Table .2). Moreover, the application of variable compression ratio engine is used to raise the CR for efficiency enhancement, but, it was reported that VCR-engine is not suitable for rural area in the developing countries, because, its displacement in engines is yet too large, and it has more maintenance and complication issues in compared to ordinary [15]. Therefore, in this study, the geomatical compression ratio (GCR) was fixed at 14, so it could be suitable for implementation in rural areas.

Existing studies have largely focused on individual use of PG or BG or on their blending with other gaseous fuels such as hydrogen, natural gas, and LPG, to analyze combustion, performance, and emissions. Only a few works have reported PG–BG blending in SI engines. For instance, Bue et al. [9] observed a 23 % power derating when switching from BG to syngas and concluded that hydrogen is more beneficial as a blending fuel. Kan et al. [75] Simulated PG–BG blends were noted, and NOx reduction and improved knock resistance were observed. However, no comprehensive study has examined the combined impact of boosted intake pressure, LIVC, and optimized spark of ignition timing (SOI) on the efficiency and brake power of PG–BG fueled SI engines.

The novelty of this research lies in integrating Miller cycle-based valve timing control (LIVC), intake boosting, and spark timing optimization for a PG–BG dual-fueled SI engine under fixed GCR operation. Unlike earlier works considering limited operational parameters or individual fuels, this study combines a quasi-dimensional thermodynamic model and response surface methodology (RSM) to simulate and optimize key variables affecting engine performance and emissions. Furthermore, the model is validated with literature data and customized using FORTRAN code, offering a replicable and practical simulation approach for rural engine applications. By considering the identified research gap and the novelty of this work, the objectives of this study are-

- To illustrate how PG-BG fueled SI engines can be made more powerful and efficient.
- To evaluate how increasing intake pressure and intake valve closure timing affect engine performance and emission metrics.
- Finding the optimum operational parameters (intake pressure, inlet valve closure timing and SOI timing) to achieve both maximum power and minimal emissions.

To accomplish the mentioned objective, TQD modeling has been conducted to simulate the performance of SI engine in order to investigate and improve the power and efficiency with low emission. On this base, keeping 14 GCR and 1500 engine rpm, the effect of operating parameters as LIVC (IVC from 60 - 85° aBDC), Start of Ignition (SOI from 15-30° bTDC), and boost intake pressure (1–2.5 bar) has been taken into consideration to evaluate the performance of equi-volume (BG/PG) SI engine. Accordingly, the simulation provides performance results to understand the effect of each parametric variable and compare one to the other. After that, the prediction of the optimal operating parameters in respect to the balance between maximizing power and efficiency and minimizing exhaust emissions of an engine. The simulation work includes the power cycle simulation of a 4-stroke engine through Fortran Code and the optimization of variables through the response surface method (RSM). Engine power, efficiency, fuel consumption, and emissions are estimated using a TQDM-based simulation in a range of operating conditions. It also involves determining combustion parameters using a two-zone burning model and validating them against experimental results from the literature. RSM includes a mathematical technique for producing an empirical model to converge minimum and maximum value, and it is very popular today due to its effectiveness and quick-solving ability [76]. Finally, it was revealed that the equi-volume blend of PG and BG can be efficiently used to run a dual-fueled mode SI engine with enhanced power and efficiency when parameters would be adjusted optimally. Further, the aforementioned research work reports a good technical route to predict SI engine performance and emissions for scholars and businesses for further research and development.

2. Materials and methodology: A thermodynamic simulation

In this study, engine performance was simulated by using the fundamental law of thermodynamics. A quasi-dimensional thermodynamic model was created with the help of basic equation of thermodynamic. In this model two zone combustion (burnt and unburnt zone) were considered. The simulation started with the closing of the inlet valve, moved through the compression stroke where the air-fuel mixture was compressed, generated a circular fire nucleus at the end of compression, propagated a turbulent flame with two zones (burnt and unburnt) until it reached the combustion point, and expanded until the exhaust valve opened. Flame surface configuration and crank angle were utilized to calculate the flame surface area and related burnt volume during and after combustion [77]. In the two-zone combustion model, heat transferred from the end gas to the walls was calculated using Anand equation [78]. It was expected that the burning inside the combustion chamber would stop when the mass of the new charge dropped to zero. The molar fraction of 12 product species (CO_2, H_2O, N_2, H_2, OH, H, NO, N, Ar, CO, O, and O_2) formed during combustion of fuel was calculated by using the 7-equilibrium equation and, one combustion equation with balancing of carbon (CO), oxygen (O), nitrogen (N), and argon. On the other hand, a rate kinetics model has been used to calculate the CO and NO concentrations for temperature with crank angle because NO and CO species are generated after combustion, which is a time-dependent parameter. Polynomial interpolations have been used to calculate the specific heats and enthalpies of individual mixture species with respect to temperature. The approximations and presumptions in the quasi-dimension thermodynamic model were recorded using Benson's [77] model, which contains the (i) fuel and air mixture input and is assumed to be homogenous. (ii) Uniform pressure inside cylinder at any time. (iii) The volume at the flame reaction areas is considered negligible. (iv) Both gases have constant specific heat. (v) In this model, there is no heat transfer between the two ((burned and unburned) zones. Heat transfer to the combustion chamber walls is modeled using the Annand equation, assuming it occurs exclusively from the burned zone. The remaining energy in the burned gases, after wall heat loss, is considered to be entirely converted into work. However, in reality, a portion of heat is also transferred from the burned zone to the unburned zone. This inter-zone heat transfer slightly reduces the net heat available for conversion into work, leading to a deviation from the ideal assumption. (vi) The unburnt gas is assumed to be iced at its initial composition. The intricate procedure configuration for SI engine performance numerical simulation is demonstrated in Fig. 1.

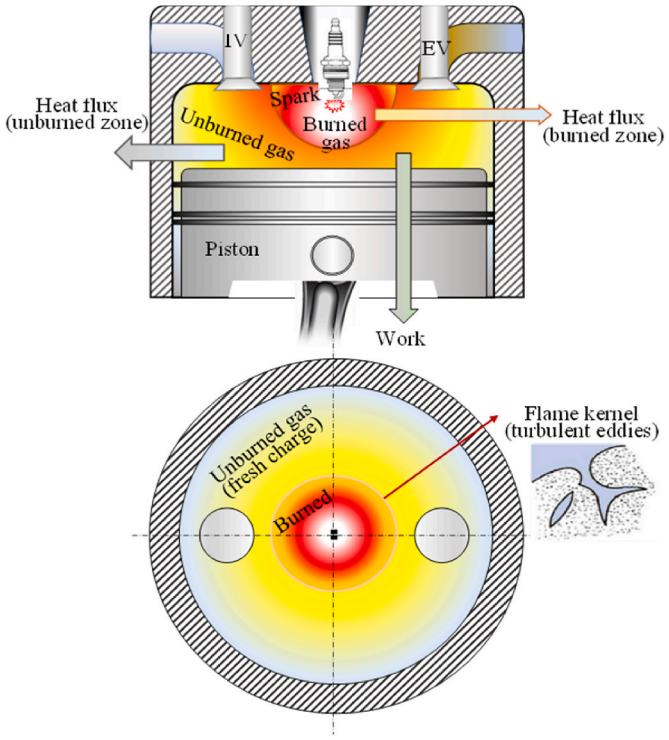

Fig. 2. Two-zones combustion chamber for engine modeling.

2.1. Compression model

The thermodynamic equation of state and compression begins when the inlet valve closes (IVC) [77,79]: The pressure within the cylinder of SI engine may be determined using a first-law of thermodynamics. Equations (1) and (2) depict the relationship between product temperature and cylinder pressure as a function of crank angle.

$$\frac{dp}{d\theta}=\left(\frac{1}{V}\right)\left[\left(\frac{R}{cv}\right)\left(\frac{dQ}{d\theta}\right)-\left(\frac{Pdv}{d\theta}\right)\left(\frac{R}{cv}+1\right)\right] \tag{1}$$

$$\frac{dT_m}{d\theta}=T_m\left(\frac{1}{V}\frac{dV}{d\theta}+\frac{1}{P}\frac{dP}{d\theta}\right) \tag{2}$$

$$\frac{dV}{d\theta}=\frac{V_c}{2}(CR-1)\left[(\sin\theta)+\frac{\sin\theta\cos\theta}{\sqrt{\frac{L^2}{a_c{}^2}-sin^2\,\theta}}\right] \tag{3}$$

Heat released from the burned zone and unburned zone to the wall can be calculated by Annand's equation [78].

$$\frac{q_h}{F}=\frac{a_c K_q}{d}(\mathrm{Re})^{b_c}(T_m-T_w)+c_c\left(T_m^4-T_w^4\right) \tag{4}$$

Where $a_c = 0.4$, $b_c = 0.7$, $c_c = -0.43\times10^{-9}$ are constant.

The work done within the piston cylinder is given by equation (5).

$$\frac{dw}{d\theta}=p\frac{dV}{d\theta} \tag{5}$$

The 4th order range kutta method is used to calculate the increasing variable in the compression stroke:

$$X_{n+1}=X_n+\frac{dX}{d\theta}\Delta\theta \tag{6}$$

2.2. Combustion with two zones

The combustion process begins after a brief ignition delay and progresses through two clearly defined regions: one comprising the burned gases and the other consisting of unburned mixture [80], as illustrated in Fig. 2. This passage describes the standard approach commonly used in quasi-dimensional models to simulate the exchange of heat and work between the burned zone (Vp) and the unburned zone (Vm). The following equations are utilized to determine the flame propagation speed and to evaluate the thermodynamic states of both zones during combustion [77,79]:

$$\frac{\mathrm{dV}}{\mathrm{d}\alpha}=\frac{\mathrm{dV_m}}{\mathrm{d}\alpha}+\frac{\mathrm{dV_p}}{\mathrm{d}\alpha};=\left(\frac{\mathrm{V_p}}{\mathrm{m_p}}-\frac{\mathrm{V_m}}{\mathrm{m_m}}\right)\frac{\mathrm{dm_p}}{\mathrm{d}\alpha}+\frac{\mathrm{m_m R_m}}{\mathrm{p}}\frac{\mathrm{dT_m}}{\mathrm{d}\alpha}+\frac{\mathrm{m_p R_p}}{\mathrm{p}}\frac{\mathrm{dT_p}}{\mathrm{d}\alpha}-\frac{\mathrm{V}}{\mathrm{p}}\frac{\mathrm{dp}}{\mathrm{d}\alpha} \tag{7}$$

$$\frac{dT_m}{d\alpha}=\frac{V_m}{m_m C_{p_m}}\left(\frac{dP}{d\alpha}\right)+\left(\frac{1}{m_m C_{p_m}}\right)\left(\frac{dQ_m}{d\alpha}\right); \tag{8}$$

$$\frac{dT_p}{d\alpha}=\frac{p}{m_p R_p}\left[\frac{dV}{d\alpha}-\left(\frac{R_p T_p}{p}-\frac{R_m T_m}{p}\right)\frac{dm_p}{d\alpha}-\frac{R_m V_m}{pc_{p_m}}\frac{dp}{d\alpha}-\frac{R_m}{pc_{p_m}}\frac{dQ_m}{d\alpha}+\frac{Vdp}{pd\alpha}\right] \tag{9}$$

$$\frac{dp}{d\alpha}=\frac{\left(1+\frac{\mathrm{c_{vm}}}{\mathrm{R_p}}\right)\mathrm{p}\frac{\mathrm{dV}}{\mathrm{d}\alpha}+\left\{(\mathrm{u_p}-\mathrm{u_m})-\mathrm{c_{v_p}}\left(\mathrm{T_p}-\frac{\mathrm{R_m}}{\mathrm{R_p}}\mathrm{T_m}\right)\right\}\frac{\mathrm{dm_p}}{\mathrm{d}\alpha}+\left\{\frac{\mathrm{c_{vm}}}{\mathrm{c_{p_m}}}-\frac{\mathrm{c_{vp}}}{\mathrm{R_p}}\frac{\mathrm{R_m}}{\mathrm{c_{p_m}}}\right\}\frac{\mathrm{dQ_m}}{\mathrm{d}\alpha}-\frac{\mathrm{dQ}}{\mathrm{d}\alpha}}{\left[\frac{\mathrm{c_{vp}}}{\mathrm{c_{p_m}}}\frac{\mathrm{R_m}}{\mathrm{R_p}}\mathrm{V_m}-\frac{\mathrm{c_{vm}}}{\mathrm{c_{p_m}}}\mathrm{V_m}-\frac{\mathrm{c_{vp}}}{\mathrm{R_p}}\mathrm{V}\right]} \tag{10}$$

$$\text{Burning rate}: \frac{dm_b}{dt}=A_f\rho_u u_T \tag{11}$$

Where A_f, = flame surface area calculated by the geometric model confirmed by Risso et al. [81], ρ_u = density, and u_T = turbulent flame velocity.

$$\text{Turbulent flame velocity}: u_T=u'+S_{l,(PG+BG)} \tag{12}$$

$$\text{turbulence intensity } u'=0.5S_p\left[1-\frac{0.5(\theta-180)}{45}\right] \tag{13}$$

Le Chatelier's Rule [82] calculates the laminar flame velocity for a dual fuel.

$$S_{L(PG+BG)}(\phi,x,T,P)=\left[\frac{1}{S_{PG}(\phi,T,P)}+\frac{1}{S_{BG}(\phi,T,P)}\right]^{-1} \tag{14}$$

Where $S_{l(PG)}$ and $S_{l(BG)}$ are the laminar combustion velocity of PG [83] and BG [84]:

$$S_{l(PG)}=(S_{ref})_{PG}\left(\frac{T_u}{T_{u,ref}}\right)^{\alpha}\left(\frac{P}{P_{ref}}\right)^{\beta} \tag{15}$$

Where constant $\alpha = 2.0$, $\beta = -0.4$, S_{ref} = laminar burning velocity in m/s 0.56–0.827(ϕ-1.186)^2 at $P_{ref} = 1$ atm and $T_{u,\ ref} = 298$ K

$$S_{L(BG)}(\varphi, x_{CO_2}, T, P) = \left[\begin{array}{l} S_{u,0} + S_{u,1}(\varphi-1) + S_{u,2}(\varphi-1)^2 \\ +S_{u,3}(\varphi-1)^3 + S_{u,4}(\varphi-1)^4 \end{array}\right] \times \left[T^{\eta_{BG}} P^{\beta_{BG}} \left(1 - \mu_1 x_{CO_2}^{(\mu_2+(\varphi-1))\mu_3}\right)\right] \quad (16)$$

T_u is the temperature of the unburned gases and Pu is the pressure, $P = \frac{P_u}{1.01}$ at 298 K and 1 bar. The constants linked to the CO_2 proportion as X_{CO2} are $\mu_{1\text{-}3}$, whereas $Su,_{1\text{-}4}$ are the coefficients of the polynomial. Constant values are given in Table 4. The following are the coefficients:

$$\eta_{BG} = \eta_0 + (\phi - 1)\eta_1 \quad (17)$$

$$\beta_{BG} = \beta_o + (\phi - 1)\beta_1 \quad (18)$$

The configuration of biogas was implemented from the study of Hinton et al. [84]. Which depicts CH_4 70 % and CO_2 30 % by volume percentage. The biogas CV (33.906 MJ/Nm^3) was calculated using 70 % of the CH_4. The configuration of PG was implemented from the work of tinaut et al. [83]. calorific value of 5947.0 kJ/Nm3 for 20 % CO, 18 % H_2, 12 % CO_2, 5 % CH_4, and 45 % N_2. Using the polynomial constant in J/kg-mol for the PG and BG composition, the internal energy of PG and BG were calculated from Ref. [85].

The internal power of biogas was determined using the following formula:

$$a_{i,BG} = Y_i f_{i,CH_4} + Y_i f_{i,CO_4} + Y_i f_{i,H_2} + Y_i f_{i,N_2} \quad (19)$$

These coefficients are referred from Ref. [85] and given in Table 5. When biogas is blended with producer gas, the combined polynomial constant for internal energy (J/kg-mol.K) is given as:

$$U_{Blend,i} = 0.5(a_{BGi})_{BG} + 0.5(U_{PGi})_{PG}$$

Molecular weight calculated by:

$$W_{BG} = 44 \times f_{CO_2} + 16 \times f_{CH_4} + 2 \times f_{H_2} + 28 \times f_{N_2}$$

$$W_{PG} = 28 \times f_{CO} + 44 \times f_{CO_2} + 16 \times f_{CH_4} + 2 \times f_{H_2} + 28 \times f_{N_2}$$

Total blended Molecular weight

$$Wt_{(BG+PG)} = W_{PG} \times (1 - f) + W_{BG} \times f$$

Correlation between the mole fraction (f) and the mass fraction (x) [87];

$$x = \frac{f.MW_{BG}}{f.MW_{BG} + (1-f)MW_{PG}}$$

The value of PG density are determined by using equation (20) in order to assess the GCV per kg mass [88]:

$$\rho_{PG} = \left[(f_1.\rho)_{CO} + (f_2.\rho)_{H_2} + (f_3.\rho)_{CH_4} + (f_4.\rho)_{CO_2} + (f_5.\rho)_{N_2}\right] \ (\mathrm{kg/Nm^3}) \quad (20)$$

where $f_{1\text{-}5}$ are the molar fractions of the producer gas compound, and $\rho_{CO} = 1.16$, $\rho_{H2} = 0.09$, $\rho_{CH4} = 0.67$, $\rho_{CO2} = 1.84$ and $\rho_{N2} = 1.16$ are the density of the compounds at NTP. The CV of producer gas equivalent to 5947.0 kJ/Nm^3, 5786.65 kJ/kg with a density equal to 1.027 kg/Nm^3 and for biogas CV equal to 23734.2 kJ/Nm^3, 29865.23 kJ/kg with density of 0.79 kg/m^3 [36] were calculated by-

Blended LHV (MJ/kg):

$$LHVt_{(PG+BG)} = x.LHV_{BG} \times (1-f)x.LHV_{PG}$$

2.3. Species formation

For 1 mol of the final product, the dual fuel (Biogas + Producer gas) and air reaction equation is as follows:

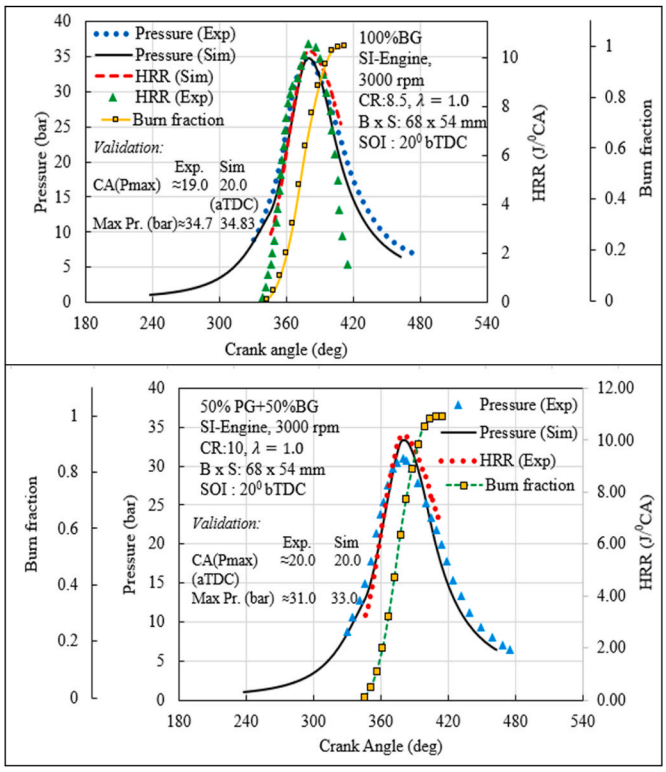

Fig. 3. Validation with the experimental results.

$$a\left[0.5\left(C_nH_mO_p\right)_{BG} + 0.5\left(C_nH_mO_p\right)_{PG}\right] + \frac{a}{\phi}\left[\left(n + \frac{m}{4} - \frac{r}{2}\right)\right]\left(O_2 + \frac{78}{21}N_2 + \frac{1}{21}Ar\right) \rightarrow \sum_{i=1}^{12} x_i \quad (21)$$

where: n, m, p, are the atom of caron, hydrogen and oxygen in fuel, respectively. And x_i denotes mole of total species products, ϕ is the equivalence ratio and a is the mole of fuel plus $1/\phi$ times the stoichiometric quantity of air.

Benson et al. [77,89] employed atomic balance equations to determine the concentrations of twelve chemical species, including CO_2, H_2, H, OH, NO, N_2, N, O_2, CO, H_2O, O, and Ar. However, the formation of CO and NO in an engine does not follow equilibrium processes. Therefore, their concentrations, as proposed by Lavoie et al. [89,90] are modeled using a Rate Kinetic Approach. The equations used to simulate NO and CO formation are presented as equations (22) and (23).

$$\frac{1}{V}\frac{d}{dt}(NO)V = 2\left(1 - \alpha^2\right)\left[\frac{R_1}{1 + \alpha\left[\frac{R_1}{(R_2+R_3)}\right]} + \frac{R_6}{1 + \left[\frac{R_6}{(R_4+R_5+R_7)}\right]}\right] \quad (22)$$

In this equation, α represents the ratio of the actual nitrogen oxide concentration to its equilibrium value, i.e., $[NO]/[NO]_e$. Here, V denotes the volume of the reaction products, and $R_{1\text{-}7}$ corresponds to the forward reaction rates for the equilibrium processes.

$$\frac{1}{V}\frac{d}{dt}(CO)V = -k_f[\mathrm{CO}][\mathrm{OH}] + k_b[CO_2][H] \quad (23)$$

where; K_f and K_b are the forward and backward rate constant respectively.

Table 3
Engine specifications for simulation.

Particular	Specification	Input variable
SI Engine Honda GX200 [9]:	Single Cylinder, 4-stroke	
Bore Diameter	68.0 mm	
Stroke	45.0 mm	
Inlet valve closing	598^0CA (58° aBDC)	60-85^{0}CA-aBDC
Exhaust valve opening	105^0CA (75^0bBDC)	
Inlet valve opening	329^0CA (31° bTDC)	
Exhaust valve closing	375^0CA (15° aTDC)	
Start of Spark Timing	20° bTDC	30-15° CA-bTDC
CR	8.5	12 (GCR)
RPM	3000	1500
Equivalence ratio	1.0	
Fuel	Biogas	50 %
	Producer Gas	50 %
Calorific value [9]	23734.2 (kJ/Nm^3)	

Table 4
Values of constant [84] (equation (16)).

$S_{u,0}$	$S_{u,1}$	$S_{u,2}$	$S_{u,3}$	$S_{u,4}$
28.0953	0.54516	−189.4896	−26.1083	524.5957
η_0	η_1	μ_1	μ_2	μ_3
2.3614	0.40855.	1.077	1.14	−0.83453
β_0	β_1			
−0.38146	−0.081554			

Table 5
Calculated internal energy coefficient (J/kmol.K) for BG and PG.

BG [100]				
$a_{1,\ BG}$	$a_{2,\ BG}$	$a_{3,\ BG}$	$a_{4,\ BG}$	$a_{5,\ BG}$
$-\ 1.6711 \times 10^8$	$-\ 1905.36$	47.58	$-\ 1.5732 \times 10^{-2}$	2.6119×10^{-6}
PG [100]				
$U_{\ PG1}$	$U_{\ PG2}$	$U_{\ PG3}$	$U_{\ PG4}$	$U_{\ PG5}$
$-\ 8.0522 \times 10^7$	*18513.24*	5.5071	$-\ 8.90276 \times 10^{-4}$	1.2105×10^{-6}

2.4. Performance variables

$$\text{Indicated work}: \frac{dw}{d\alpha} = p\frac{dV}{d\alpha},\ W_d = \int_{IVC}^{EVO}\left[P(\alpha)\ \frac{dV}{d\alpha}\right]d\alpha \tag{24}$$

$$\text{Indicated mean effective pressure}: IMEP(bar) = \frac{W_d(kJ)/100}{V_s(m^3)} \tag{25}$$

$$\text{Indicated power}: IP\ (kW) = \frac{W_d\ (kJ)}{120}\ N;\ \text{N is rpm} \tag{26}$$

$$\text{Indicated thermal efficiency}: \eta_i = \frac{IP\ (kW)}{m\ (kg/s).\ CV(kJ/kg)} \tag{27}$$

$$\text{Brake Power}: BP = \frac{BMEP.\ V_s\ .\ N}{120} \tag{28}$$

3. Results and discussion

3.1. Validation of quasi dimensional thermodynamic model

The developed quasi-dimensional thermodynamic model was validated against experimental data reported in the literature. Bui et al. [91] conducted a study to validate numerical simulation models by comparing key combustion parameters such as cylinder pressure vs crank angle graph and heat release rate vs crank angle, demonstrating good agreement between experimental and simulated results. In this study, Fig. 3 presents the validation for a pure biogas and fuel blend comprising 50 % producer gas and 50 % biogas. The engine specifications used in the simulation are detailed in Table 3. The comparison indicates that the simulated trends for the pure biogas and biogas–producer gas blend closely follow the experimental results. Minor deviations can be attributed to cycle-to-cycle variation and modeling assumptions. The most significant peak pressure deviation observed was 6.06 %, corresponding to a crank angle difference of 10° CA for the 50–50 fuel blend. This level of agreement supports the predictive capability of the developed simulation model under the considered operating conditions.

3.2. RSM approach

The spark ignition (SI) engine's performance analysis parameter was investigated through the use of the central composite design (CCD) statistical method. It is frequently used in response surface methodology. RSM is a set of geometric and mathematical methods that help create predictive models, refine and optimize process parameters, and determine how various influencing elements interact [92]. The RSM method is appropriate for a rectangular surface and helps analyze the connection between the parameters and optimize the process parameters with the smallest number of repetitions. Fitting a quadratic surface is a good use for the RSM approach, This also helps with parameter analysis and optimizing process parameters with the fewest trials needed. Three main steps comprise the RSM optimization technique: First, statistical trial planning; second, mathematical model coefficient estimation; and third, response predictions and model suitability assessment [93]. In this investigation, three independent variables,

Table 6
Fuel performance data for RSM optimization.

S. No.	Pressure (bar)	SOI (CA)	LIVC (CA)	IP (kW)	ITE (%)	IMEP (bar)	BSEC (MJ/kg)	CO (vol%)	NO (ppm)
1.	1	705	600	1.84	25.73	7.53	16.910	0.45	344.6
2.	1	705	625	1.51	27.3	6.2	16.687	0.44	270.9
3.	1	697.5	612.5	1.78	27.8	7.28	15.767	0.52	834.7
4.	2.5	705	600	4.74	26.45	19.3	14.582	0.38	519.1
5.	2.5	690	600	5.25	29.26	21.4	13.090	0.55	2081.1
6.	1.75	697.5	600	3.55	28.3	14.51	13.964	0.45	1160.9
7.	1	690	625	1.6	28.65	6.5	15.713	0.63	1882.8
8.	2.5	705	625	3.9	28.08	15.9	13.955	0.38	485.9
9.	1.75	705	612.5	2.97	26.5	12.14	15.212	0.4	443.5
10.	1	690	600	1.97	27.53	8.06	15.589	0.62	2066.3
11.	2.5	697.5	612.5	4.65	29.03	19	13.305	0.45	1222.4
12.	2.5	690	625	4.23	30.43	17.3	12.785	0.54	2080.1
13.	1.75	690	612.5	3.23	28.8	13.19	13.865	0.58	2122.1
14.	1.75	697.5	625	2.9	29.72	11.81	13.608	0.47	1006.3
15.	1.75	697.5	612.5	3.21	28.58	13.09	13.980	0.47	1094.2

Table 7
ANOVA analysis for response model.

Response parameter	Sum of Square	Degree of freedom	Mean Square	F-value	P-value	Adjusted R^2	Predicted R^2
IP (kW)	21.25	9	2.36	2637.03	<0.0001	0.9994	0.9964
ITE (%)	23.23	9	2.58	615.95	<0.0001	0.9975	0.9920
IMEP (bar)	352.88	9	39.21	2700.96	<0.0001	0.9994	0.9970
BSEC (MJ/kWh)	23.60	9	2.62	695.94	<0.0001	0.9978	0.9929
CO (vol%)	0.0916	9	0.0102	148.63	<0.0001	0.9896	0.9481
NO (PPM)	6.904E+06	9	7.671E+05	132.28	<0.0001	0.9883	0.9571

intake pressure (bar), spark of ignition timing (bTDC), and inlet valve closing timing (aBDC), were selected for the statistical simulation design. it is imperative to optimize these input parameters. The ranges of input variables vary according to previous studies, computations, and engine limitations.

This study used response surface methodology to optimize outcome data based on FORTRAN simulation during a process. The 15 test data of the dual fuel for performance and emissions of SI engine responses are demonstrated in Table 6. The entire polynomial 2nd order equation contributes as the regression model equation in RSM. Which can be written as equation (29).

$$Y = C_0 + \sum_{i=1}^{n} C_i X_i + \sum_{i=1}^{n} C_{ii} X_i^2 + \sum_{i<j=1}^{n} C_{ij} X_{ij} + \varphi \quad (29)$$

where C_0 = regression constant, Ci = linear constant, Cii = quadratic constant, Cij=interaction effects coefficient.

The coded variables X_i and X_j are separate variables.

RSM has been used to determine the correlation between intake and response parameters, which are obtained using FORTRAN code software, and also used to formulate an appropriate forecast. Using the regression equations provided in (24–39), the statistical importance of the regression model for each output was ascertained at a 95 % confidence level. The number of samples, probability level, and detected inconsistency in the sample all influence the response surface methodology margin of error, establishing confidence. Following optimization, the simulation test results and projections showed a high degree of promise, with an error of less than 5 %.

3.3. Analysis of variance for responses

The difference between the exact and projected values was examined to study the numerical accuracy of this model. The analysis of variance results about the importance and predictive precision of the associated computational model terms are shown in Table 7. The entire regression equation is subject to a statistical significance test called the F value. The calculated variance is divided by the unexplained variance to obtain the F-value. In regression analysis, the p-value indicates the statistical significance of the relationship between the observed and predicted outputs. The F-value ranges from 0 to infinity, with higher values suggesting a better-fitting model. Conversely, the p-value lies between 0 and 1, where lower values signify a more statistically significant model. The F-values demonstrated the significance of every response model near infinity and P-values close to zero (<0.05). R^2 should be high, close to 1, and there must be a reasonable degree of agreement with adjusted R^2. The R^2 value was also calculated for the total inconsistency of responses based on the input parameters. Table .7 shows that R^2 values were higher and reached a value of 0.99, implying that the proposed model has greater accuracy. The other authors [94–96] find analogous higher values of R^2 (>0.99) for the statistical model.

Using the RSM, the inlet pressure, spark timing, and inlet valve closing timing were used to forecast the quadratic function of the output response. Equations 30–35 illustrate how the quadrate response model was established using the regression equation.

$$\text{IP (kW)} = -746.36236 + 20.90057\,Pr + 2.44462\,SOI - 0.355658\,LIVC - 0.013778\,Pr * SOI - 0.015467\,Pr * LIVC + 0.000293\,SOI * LIVC + 0.016790\,Pr^2 - 0.001877\,SOI^2 + 0.000124\,LIVC^2 \quad (30)$$

$$\text{ITE(\%)} = -6387.13459 + 32.07731Pr + 22.10598SOI - 4.21270LIVC - 0.044667Pr * SOI + 0.001467\,Pr*LIVC + 0.001213SOI*LIVC - 0.282469Pr^2 - 0.016425SOI^2 + 0.002791LIVC^2 \quad (31)$$

$$\text{IMEP (bar)} = -3057.42508 + 86.39733\,Pr + 9.93660SOI - 1.37165LIVC - 0.059333\,Pr * SOI - 0.061467\,Pr * LIVC + 0.001240\,SOI * LIVC + 0.080000\,Pr^2 - 0.007644\,SOI^2 + 0.000416\,LIVC^2 \quad (32)$$

$$\text{BSEC(MJ/kg)} = +4.01425E{+}06 - 4092.77237Pr - 13378.25331SOI + 2104.71907\,LIVC + 8.12578\,Pr * SOI - 11.10293\,Pr * LIVC - 0.890773\,SOI * LIVC + 999.70963\,Pr^2 + 10.03132\,SOI^2 - 1.20415\,LIVC^2 \quad (33)$$

$$\text{CO (vol\%)} = +171.04666 - 0.535037\,Pr - 0.541933\,SOI + 0.074947\,LIVC + 0.000667\,Pr * SOI - 0.000133\,Pr * LIVC - 0.000013\,SOI * LIVC + 0.029630\,Pr^2 + 0.000385\,SOI^2 - 0.000053LIVC^2 \quad (34)$$

$$\text{NO (PPM)} = +1.78476E{+}06 - 4057.57235Pr - 4964.48200\,SOI - 31.98289LIVC + 3.94222\,Pr * SOI + 2.97333\,Pr * LIVC + 0.103467\,SOI * LIVC - 108.96790\,Pr^2 + 3.43032\,SOI^2 - 0.039964\,LIVC^2 \quad (35)$$

3.4. Performance analysis

The performance evaluation of an internal combustion engine is a decisive parameter that signifies how much the chemical energy present in the fuel is transformed into valuable work. This perspective considers the level of effectiveness by examining key factors such as IP, ITE, IMEP, and BSEC.

The term indicated power refers to the quantity of power produced through fuel combustion within the cylinder [97]. Fig. 4(a) exquisitely delineates the combined influence of SOI, LIVC, and intake boost pressure on the indicated power. Fig. 4(a) demonstrates that the intake boost pressure exhibits the most significant fluctuation in the indicated power. When intake boost pressure increases, the IP is enhanced because of increasing the fuel consumption, leading to the temperature and pressure of cylinder [98,99]. The increase of intake boost pressure from 1 bar to 2.5 bar results in an IP increase of approximately 166.49 % at constant 15° bTDC spark timing and 60° aBDC inlet valve closing timing. IP increases because more air-fuel mixture is forced into the cylinder by increasing the intake pressure, leading to better combustion and higher fuel power. It is also noted from Fig. 4(a) that the trend of indicated power slightly decreases when LIVC timing is increased with respect to the intake pressure. This effect is caused by reducing the trapped volume. When R. Wang et al. [98] compared the miller cycle to the otto cycle, they also discovered an analogous power inclination. The maximum value of indicated power obtained at the simulation of 60° aBDC-LIVC, 30° bTDC-spark timing and 2.5 intake boost pressure is 5.25 KW.

ITE refers to the ratio between the indicated power (IP) and the needed heat energy of fuel [100]. Fig. 4(b) demonstrates the collective impacts of the spark timing, intake pressure and inlet valve closing timing. As illustrated in Fig. 4(b), the ITE increases slowly to the certain

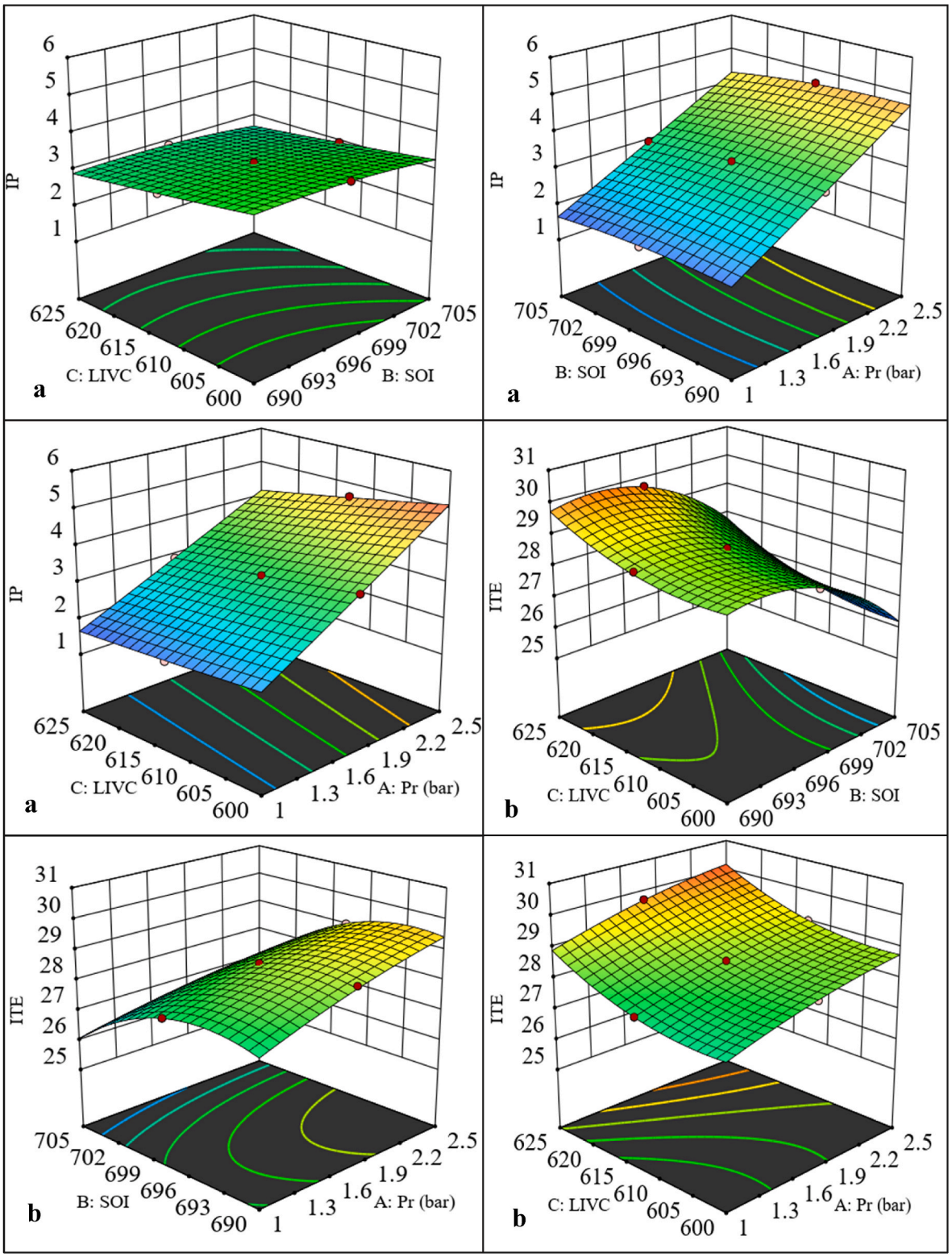

Fig. 4. Effect of decision parameters on (a) IP and (b) ITE.

LIVC increment and then increases proportionally with the LIVC increment. This is because, as the LIVC crank angle increases, the trapped volume of charge reduces, subsequently, the expansion ratio becomes higher in compared to the actual compressor ratio attained at the inlet valve close. This enhances the net work done, thus efficiency improves with LIVC increment at given fuel intake. Moreover, this behaves as inlet valve operated Miller cycle. Moreover, the clarification regarding variation of in-cylinder pressure with LIVC has been included in the supplementary file. Similar trends were also found by Prajapati et al. [101]. ITE increases with advancing the spark timing from 705° CA (15° bTDC) to 690° CA (30° bTDC). When the spark timing is increased, combustion duration is also increased due to increasing flame propagation and combustion efficiency, and maximum efficiency is achieved when most of the combustion happens near TDC [102]. Excessively

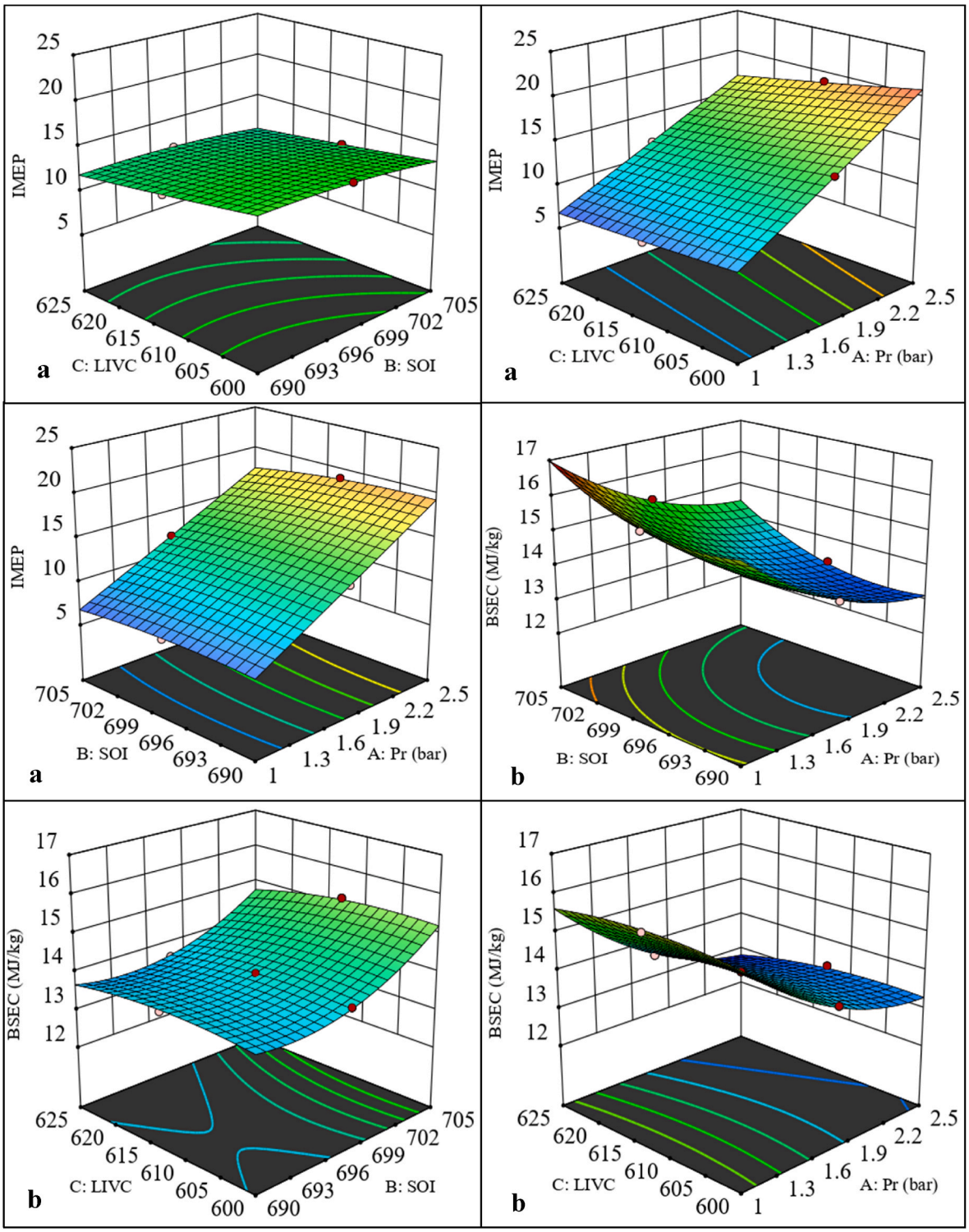

Fig. 5. Effects of Decision parameter on (a) IMEP (b) BSEC.

delayed spark timing reduces power and efficiency by allowing combustion to continue into the expansion phase, producing less work output and more compression work [103]. The surface plots show that ITE is increased by increasing the intake pressure. This is attributed to enhanced combustion efficiency and reduction ignition lag [104]. Intake pressure is increased from 1 bar to 2.5 bar, resulting in a 4.42 % increase in ITE. A similar trend was also observed by Garcia et al. [105]. The maximum ITE was obtained at the run of 85° aBDC LIVC, 30° bTDC and 2.5 bar intake boost pressure was 30.43 %.

IMEP is a significant parameter in evaluating the performance of various engines, as it provides a measure of engine power that is independent of engine size or displacement volume [100]. Fig. 5(a) illustrates the concurrent influence of SOI timing, intake pressure, and LIVC on the IMEP. It is evident from Fig. 5(a) that the intake boost pressure produces the most significant impact on the IMEP. The rise in intake pressure leads to a linear escalation in IMEP. The observed increase can be due to the concurrent rise in-cylinder temperature, pressure, and flame propagation. When the intake boost pressure is raised from 1 bar

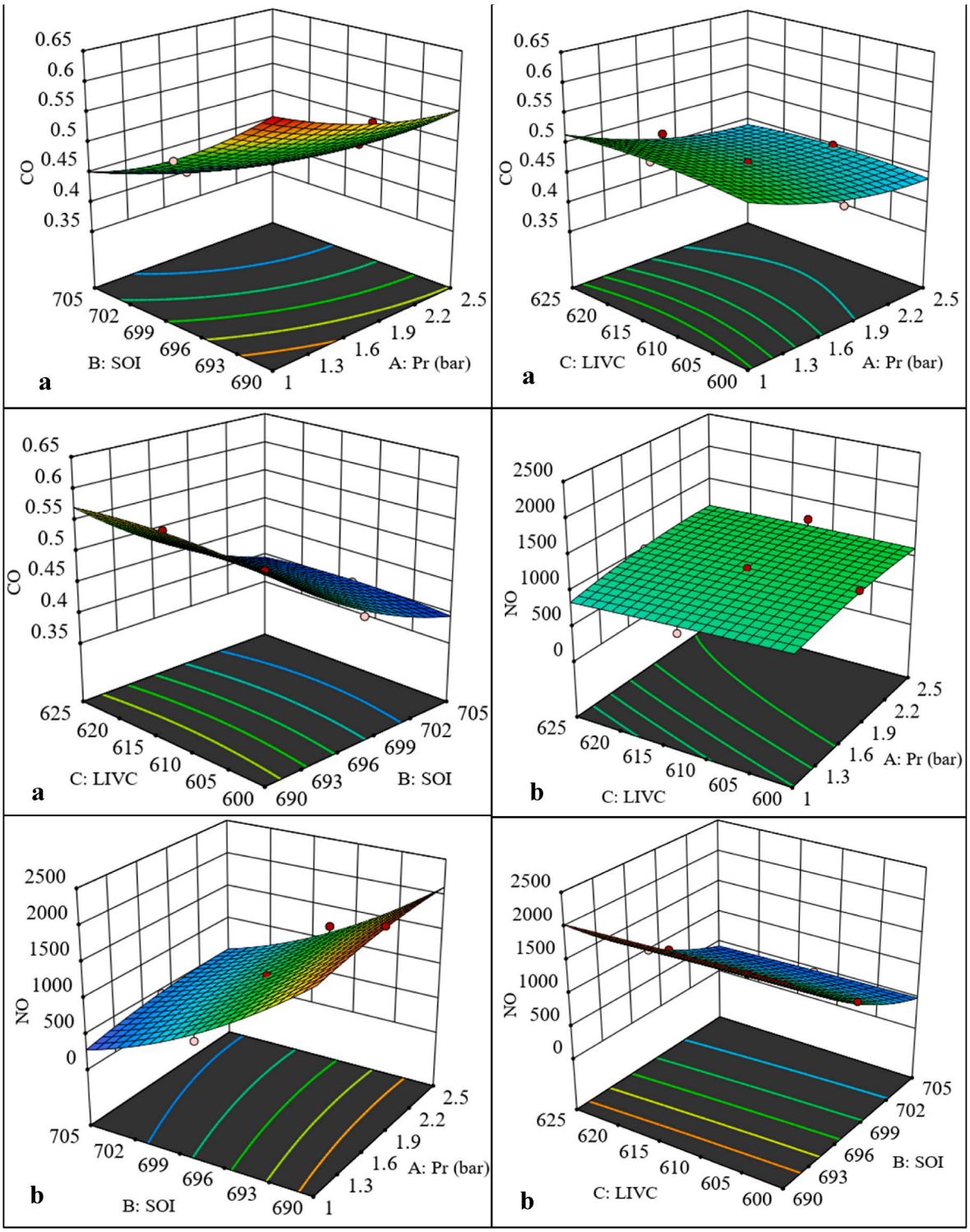

Fig. 6. Effects of Decision parameter on (a) CO and (b) NO.

to 2.5 bar, the IMEP increases by 165.50 % at a constant 15° bTDC SOI and 60° aBDC LIVC. As the inlet valve closing time increases with spark timing, the IMEP decreases. This decrease in IMEP is due to the reduction in the combustion duration, leading to incomplete combustion. The surface plots indicate that advancing the spark timing increases IMEP; specifically, IMEP improves by approximately 9 % when the SOI is advanced from 15° to 30° bTDC at an inlet pressure of 2.5 bar and a LIVC timing of 60° aBDC. This improvement is attributed to better combustion phasing, allowing the pressure to rise closer to TDC. Under producer gas–biogas dual-fuel conditions, this effect is more pronounced because the lower reactivity of producer gas benefits significantly from earlier ignition, enabling more complete combustion and higher in-cylinder pressure development. The maximum value of IMEP noticed at run of 60° aBDC LIVC, 30° bTDC spark timing and 2.5 bar intake pressure was 21.4 bar.

Brake-specific energy consumption (BSEC) represents the amount of energy required to generate 1 kW of power, calculated by multiplying the brake-specific fuel consumption (BSFC) with the gross calorific value

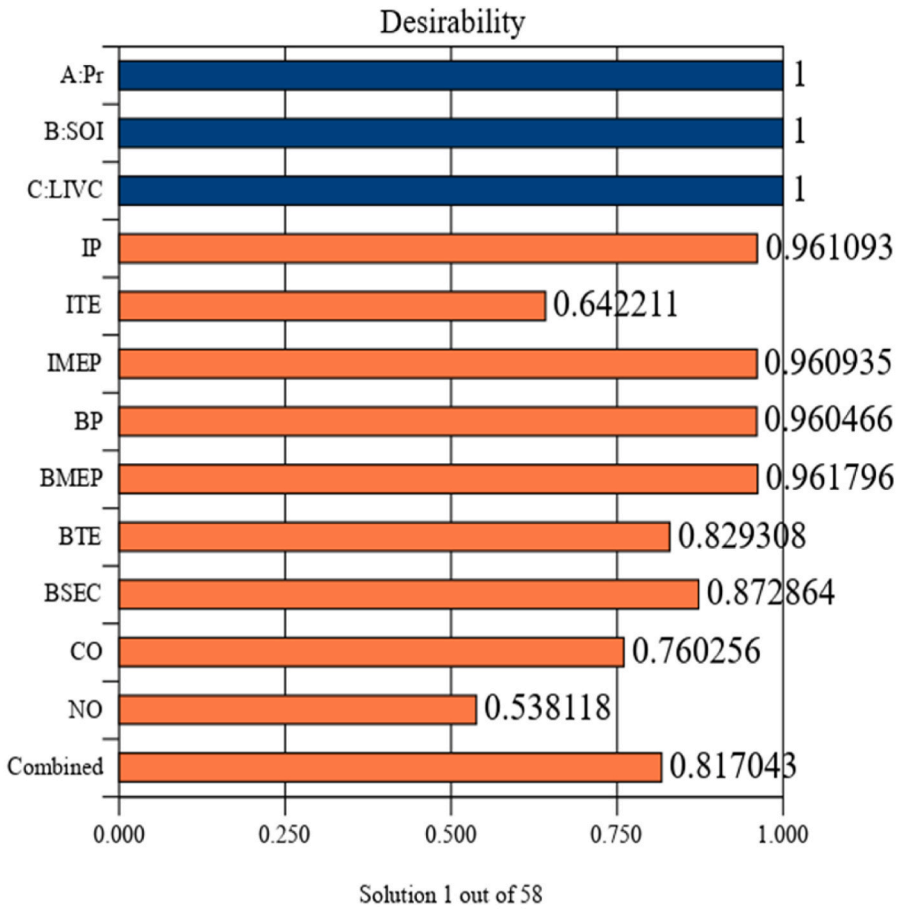

Fig. 7. Compound desirability of intake and output parameter.

(GCV) [106]. Fig. 5(b) illustrates the combined influence of spark timing, intake pressure, and LIVC on BSEC. The figure reveals that intake pressure has the most significant effect on BSEC variation. As intake boost pressure increases, BSEC shows a downward trend due to enhanced peak pressure and temperature, which promote more complete combustion. Specifically, BSEC is reduced by 16.3 % when intake pressure rises from 1 bar to 2.5 bar. SOI also affects BSEC, advancing the spark ignition from 15° to 30° bTDC leads to a 5.8 % decrease in BSEC. This reduction is attributed to the prolonged combustion duration resulting from advanced ignition, improving combustion efficiency. Additionally, a slight decline in BSEC is observed with increased LIVC timing. This is due to a reduction in trapped volume, limiting the amount of fuel entering the combustion chamber. The lowest BSEC value of 12.78 MJ/kWh was achieved at 85° aBDC LIVC, 30° bTDC spark timing, and 2.5 bar intake pressure.

3.5. Emission analysis

The concentration of CO and NO has been measured using the rate kinetic approach. The incomplete combustion of fuels produces the colorless, odorless gas known as carbon monoxide (CO). The synchronized impact of spark timing, LIVC and intake pressure on CO are shown in Fig. 6(a). It is observed from Fig. 6(a) that delaying the inlet valve close timing decreases CO emission because it increases the volumetric efficiency, which allows additional oxygen in the piston cylinder. When this oxygen combines with CO, CO_2 is created. A similar tendency was also noted [107,108]. It is also clear from Fig. 6(a) that CO emission decreases with delaying of SOI towards TDC. It is decreasing because of increasing the pressure and temperature of cylinder after combustion [109,110]. Due to spark retarding it has two reasons for decreasing the CO formation. Firstly, a longer mixing time reduces the presence of fuel-rich zones where CO is typically formed. Secondly, the higher charge temperature during the expansion stroke promotes the oxidation of CO to CO_2 in the post-flame oxidation. Both effects contribute to the reduction in CO emissions. The favorable conditions for low CO emission were found to be 15° bTDC. The trend of CO emission is decreasing with increased intake pressure because of increased combustion efficiency. During the final combustion phases in IC engines, the conversion of unconverted CO to CO_2 takes place through an intermediate step [111]. The minimum CO formation was obtained at 2.5 bar intake pressure, 15° bTDC spark timing, and 85° aBDC LIVC timing, yielding a value of 0.38 % vol. This is significantly lower than the 0.74 % vol reported by Bui et al. [112] for a biogas–hydrogen fueled SI engine and 1.1 % reported by Bui et al. [113] for a producer of gas diesel fueled CI engines. The simulated CO emission is 13.51 g/kWh, which is slightly above the Euro VI standard [114]. However, these emissions can be further reduced by employing a catalytic converter, thereby enabling compliance with Euro VI emission standards.

NO is produced by the SI engine's post-burn and flame front gaseous forms. NO formation is primarily influenced by the type of fuel, gas temperature, oxygen concentration, and reaction duration during combustion [115]. The concurrent influence of LIVC timing, SOI timing, and intake pressure on NO emission at an exhaust valve open in a part-per-million (ppm) level is shown in Fig. 6(b). Fig. 6(b) illustrates that delaying the SOI timing (shifting spark toward TDC) significantly reduces NO formation. This trend can be attributed to the reduction in peak in-cylinder pressure and temperature when ignition occurs closer to TDC. As combustion is initiated later in the expansion stroke, the available time for heat accumulation is shortened, leading to lower overall combustion temperatures. Since thermal NO formation

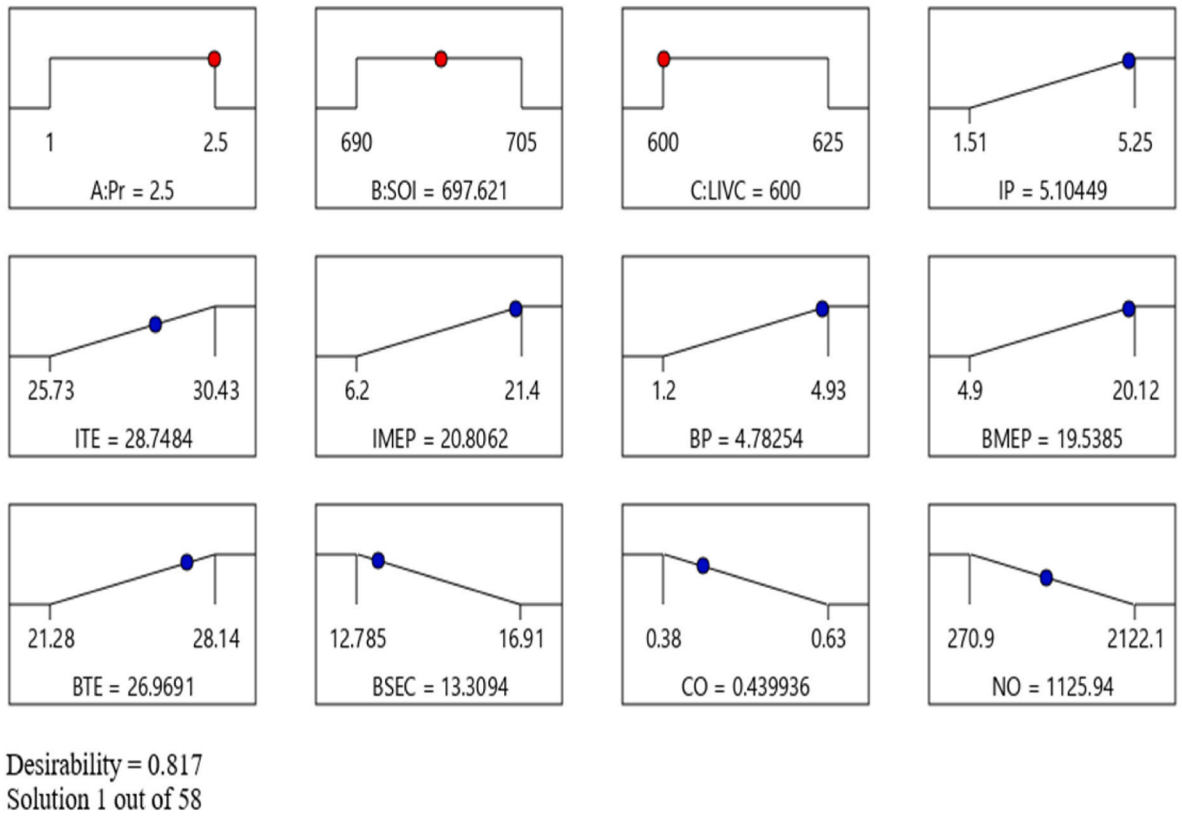

Fig. 8. Optimal value of intake and output variables.

Table 8
Optimum condition validated with simulation in error %.

	IP kW	ITE (%)	IMEP bar	BSEC MJ/kWh	CO (% vol.)	NO (ppm)
Optimized run	5.10	28.74	20.80	13.30	0.43	1125.94
Test run	5.15	28.72	21.03	13.35	0.44	1149.4
Error%	0.98	0.06	1.10	0.37	20.32	2.08

predominantly follows the Zeldovich mechanism, which is highly sensitive to temperature, suppressing peak temperature directly results in reduced NO emissions. Furthermore, delayed combustion promotes more incomplete oxidation due to the shorter high temperature residence time. This combination of effects further suppresses thermal NO production [116]. These patterns are also seen in experimental works [43,117]. It is also observed from Fig. 6(b) that increasing the intake pressure leads to increased NO formation, primarily because higher pressure results in higher in-cylinder temperatures, which in turn promote NO production. A similar trend was also reported by Mandeep et al. [118] and Mustafa et al. [119]. It can be seen in Fig. 6(b) that increasing the inlet valve closure timing decreases NO emissions due to the increased oxygen concentration in the combustion chamber. Additionally, the use of low-calorific-value gaseous fuels such as producer gas characterized by high levels of N_2 and CO_2—helps suppress NO formation by lowering peak flame temperature and limiting the availability of free oxygen during combustion. The minimum magnitude of NO emission was 270.9 ppm at 85° aBDC LIVC timing, 15° bTDC spark timing, and 1 bar inlet pressure. The simulated NO emission is 1.54 g/kWh, which is close to the Euro VI standard [120]. It can be further reduced by employing a catalytic converter so NO emission comes under Euro VI standard.

Table 9
Comparison of results from the previous study.

Parameter/Response	Previous study [121] (pure biogas)	Current study
Equivalence ratio	0.83	1.0
Spark timing	Variable (33–47°)	Variable (15–30° bTDC)
Inlet valve closing timing	–	Variable (60–85°aBDC)
Intake boost pressure	WOT (Maximum air fuel intake)	Variable (1.0–2.5 bar)
Brake Power	2.65 kW	4.78 kW
Brake thermal efficiency	26 %	26.96 %
Brake specific fuel consumption	0.81 kg/kW-h	0.78 kg/kW-h
CO emission	0.74 vol% [112]	0.43 vol%
NO emission	1192 ppm [112]	1125 ppm

3.6. Response optimization

A desirability function approach was employed to maximize BP and BTE and minimize BSFC, BSEC, CO, and NO emissions to determine the best conditions for the various runs. A greater value of desirability indicated an advanced level of accuracy. The excellent desirability was selected as one. The multi-objective optimization results indicate optimal choices with desirability values quite close to one. Fig. 7 shows the desirable values of the numerical factors along with the correlating output responses. The various parameters collectively contribute to achieving a favorable outcome across all the response variables, as indicated by a high combined desirability value of 0.817. As shown in Fig. 8, the optimal input conditions are an intake boost pressure of 2.5 bar, spark timing of 22.763° bTDC, and LIVC timing of 60° aBDC. Under these conditions, the predicted optimal values for IP, ITE, IMEP, BSEC, CO, and NO emissions are 5.10 kW, 28.78 %, 20.80 bar, 13.30 MJ/kWh,

0.439 vol%, and 1125.9 ppm, respectively. Notably, the simulated CO and NO emissions are lower than those reported by Bui et al. [112], who found optimum values of 0.74 % CO and 1192 ppm NO for a hydrogen–biogas–fueled SI engine. The comparison of the current study with a pure biogas-fueled SI engine has been presented in Table 9. The % error results for the RSM-optimized values verified compared to the simulated test run are shown in Table 8. All error percentages were found to be less than 5 %, indicating that the optimal parameter values and the outcomes of the confirmation tests are both acceptable and reliable.

4. Conclusion

Numerical simulation and flexible optimization were used in this research to determine the best response to the performance and emission parameters of an SI engine running on blends of PG and BG. To achieve this, a quasi-dimensional computational simulation model was first created using FORTRAN syntax. Then, the output of the computational simulation model was verified using the experimental cylinder pressure and crank angle graph from a previous study. Then, the working conditions of the BG-PG dual fuel SI engine, including inlet pressure, spark ignition timing, and inlet valve closure timing, were examined using this model to calculate the impact of these input parameters on the engine performance and emissions. Subsequently, RSM-Design Expert simulation techniques were utilized to optimize operating variables with the objective of minimizing BSEC, NO, and CO emissions while maximizing IP and ITE. The succeeding is a key finding of this study.

- A quasi-dimensional computational thermodynamic model that simulates the performance and emissions of a single-fuel SI engine has been developed and successfully validated.
- It was found that the reaction of output variables can be potentially reliably predicted through regression models constructed from the analysis of variance data.
- The RSM optimizer was used to determine the optimal values for the operating variables late inlet valve closure timing, spark timing, and intake pressure were 60° aBDC, 22.38° bTDC, and 2.5 bar, correspondingly.
- The optimum values for IP, ITE, IMEP, BSEC, CO, and NO are 5.10 kW, 28.78 %, 20.80 bar, 13.30 MJ/kWh, 0.439 vol%, and 1125.9 ppm, respectively.
- Brake power can be increased from 1.2 to 4.93 kW, when intake pressure raised from 1 to 2.5 bar by adjusting the LIVC and SOI.
- The total composite desirability of all the responses was 0.81, indicating a favorable outcome.

In conclusion, the current model has proven to be useful implement for the direction of investigation with less time and fewer sources regarding authentication, estimation, and optimization. It may eventually be used for other several kinds of gaseous fuel and its mixtures. However, it was discovered that PG and biogas blends were profitable sources of power production. It has been discovered that considerable trade-offs between power and emissions are caused by changes in intake pressure, spark of ignition timing, and inlet valve closure timing. The findings demonstrate that combining producer gas and biogas as dual fuel in the SI engine reduces CO and NO emissions at late inlet valve closing while also improving engine efficiency. In the future, studies utilising equivalency ratio and late inlet valve closure as variable parameters at higher crank degrees may be carried out. Additionally, this study will provide an appropriate platform for researchers to incorporate new gaseous fuel and operational variables for various performance enhancements.

CRediT authorship contribution statement

Lawalesh Kumar Prajapati: Writing – original draft, Visualization, Software, Methodology, Investigation, Conceptualization. **Jeewan Vachan Tirkey:** Writing – review & editing, Validation, Supervision, Software, Methodology, Conceptualization.

Declaration of competing interest

The authors declare that they have no known competing financial interests or personal relationships that could have appeared to influence the work reported in this paper.

Acknowledgment

We extend our heartfelt appreciation to the Department of Mechanical Engineering, IIT BHU Varanasi for their unwavering support and provision of the essential resources required for this research. The insights and assistance from the members of the IC engine lab were crucial to the positive completion of this project.

Appendix A. Supplementary data

Supplementary data to this article can be found online at https://doi.org/10.1016/j.biombioe.2025.108037.

Data availability

Data will be made available on request.

References

[1] A. Aghahosseini, et al., Energy system transition pathways to meet the global electricity demand for ambitious climate targets and cost competitiveness, Appl. Energy 331 (2023) 120401.
[2] J. Webb, H.N. de Silva, C. Wilson, The future of coal and renewable power generation in Australia: a review of market trends, Econ. Anal. Pol. 68 (2020) 363–378.
[3] D. Pudasainee, V. Kurian, R. Gupta, Coal: past, present, and future sustainable use, Future Energy (2020) 21–48.
[4] I. Abada, M. Othmani, L. Tatry, An innovative approach for the optimal sizing of mini-grids in rural areas integrating the demand, the supply, and the grid, Renew. Sustain. Energy Rev. 146 (2021) 111117.
[5] J. Leary, et al., Battery-supported eCooking: a transformative opportunity for 2.6 billion people who still cook with biomass, Energy Policy 159 (2021) 112619.
[6] E.M. Bibra, et al., Global EV Outlook 2021: Accelerating Ambitions Despite the Pandemic, 2021.
[7] A. Nurdiawati, T.K. Agrawal, Creating a circular EV battery value chain: end-of-life strategies and future perspective, Resour. Conserv. Recycl. 185 (2022) 106484.
[8] A. Malik, S. Mohapatra, Biomass-based gasifiers for internal combustion (IC) engines—a review, Sadhana 38 (2013) 461–476.
[9] V.G. Bui, et al., Flexible syngas-biogas-hydrogen fueling spark-ignition engine behaviors with optimized fuel compositions and control parameters, Int. J. Hydrogen Energy 48 (18) (2023) 6722–6737.
[10] V.G. Bui, et al., Optimizing operation parameters of a spark-ignition engine fueled with biogas-hydrogen blend integrated into biomass-solar hybrid renewable energy system, Energy (Calg.) 252 (2022) 124052.
[11] P. Bandgar, S. Jain, N. Panwar, A comprehensive review on optimization of anaerobic digestion technologies for lignocellulosic biomass available in India, Biomass Bioenergy 161 (2022) 106479.
[12] M.R. Al Mamun, S. Torii, Anaerobic co-digestion of biodegradable biomass for biomethane generation, J. Jpn. Inst. Energy 94 (6) (2015) 588–593.
[13] R. Kapoor, et al., Advances in biogas valorization and utilization systems: a comprehensive review, J. Clean. Prod. 273 (2020) 123052.
[14] P. Tamang, et al., Free nitrous acid (FNA) pretreatment enhances biomethanation of lignocellulosic agro-waste (wheat straw), Energy (Calg.) 264 (2023) 126249.
[15] E.-C. Kwon, et al., Performance of small spark ignition engine fueled with biogas at different compression ratio and various carbon dioxide dilution, Fuel (Guildf.) 196 (2017) 217–224.
[16] A. Golmakani, et al., Advances, challenges, and perspectives of biogas cleaning, upgrading, and utilisation, Fuel (Guildf.) 317 (2022) 123085.
[17] P. Gupta, C. Kurien, M. Mittal, Biogas (a promising bioenergy source): a critical review on the potential of biogas as a sustainable energy source for gaseous fuelled spark ignition engines, Int. J. Hydrogen Energy 48 (21) (2023) 7747–7769.
[18] S.K. Hotta, et al., Ignition timing and compression ratio as effective means for the improvement in the operating characteristics of a biogas fueled spark ignition engine, Renew. Energy 150 (2020) 854–867.

[19] B. Bharathiraja, et al., Biogas production–A review on composition, fuel properties, feed stock and principles of anaerobic digestion, Renew. Sustain. Energy Rev. 90 (April) (2018) 570–582.
[20] C. Liu, et al., Biogas production and microbial community properties during anaerobic digestion of corn stover at different temperatures, Bioresour. Technol. 261 (2018) 93–103.
[21] V.G. Bui, et al., Hydrogen-enriched biogas premixed charge combustion and emissions in direct injection and indirect injection diesel dual fueled engines: a comparative study, J. Energy Resour. Technol. 143 (12) (2021) 120907.
[22] B. Deepanraj, V. Sivasubramanian, S. Jayaraj, Multi-response optimization of process parameters in biogas production from food waste using Taguchi–Grey relational analysis, Energy Convers. Manag. 141 (2017) 429–438.
[23] K. Obaideen, et al., Biogas role in achievement of the sustainable development goals: evaluation, Challenges, and Guidelines, J. Taiwan Inst. Chem. Eng. 131 (2022) 104207.
[24] D. Wu, et al., Commercial biogas plants: review on operational parameters and guide for performance optimization, Fuel (Guildf.) 303 (2021) 121282.
[25] A. Chauhan, et al., Agricultural crop residue based biomass in India: potential assessment, methodology and key issues, Sustain. Energy Technol. Assessments 53 (2022) 102552.
[26] Shahin, A.M., et al., A Mini Review on Pyrolysis and Anaerobic Digestion: an Optional Approach to Enhance Energy and Valueproduct Yields from Waste of Food Waste Processing.
[27] R. Singh, et al., Strategies for selection of thermo-chemical processes for the valorisation of biomass, Renew. Energy 98 (2016) 226–237.
[28] H. Siddiqui, et al., Revamping downdraft gasifier to minimize clinker formation for high-ash garden waste as feedstock, Bioresour. Technol. 266 (2018) 220–231.
[29] R. Raj, D.K. Singh, J.V. Tirkey, Gasifier-engine performance analysis using Co-gasification of mahua wood waste and saw-dust briquette blend: an experimental and optimization approach, Biomass Conver. Biorefin. (2023) 1–24.
[30] D. Prando, et al., Characterisation of the producer gas from an open top gasifier: assessment of different tar analysis approaches, Fuel (Guildf.) 181 (2016) 566–572.
[31] A. Wiyono, et al., Design, development and testing of integrated downdraft gasifier and multi IGCS system of MSW for remote areas, Case Stud. Therm. Eng. 20 (2020) 100612.
[32] A.N. Rollinson, J.M. Oladejo, 'Patented blunderings', efficiency awareness, and self-sustainability claims in the pyrolysis energy from waste sector, Resour. Conserv. Recycl. 141 (2019) 233–242.
[33] R. Raj, D.K. Singh, J.V. Tirkey, Performance simulation and optimization of SI engine fueled with peach biomass-based producer gas and propane blend, Therm. Sci. Eng. Prog. 41 (2023) 101816.
[34] N. Homdoung, N. Tippayawong, N. Dussadee, Performance and emissions of a modified small engine operated on producer gas, Energy Convers. Manag. 94 (2015) 286–292.
[35] S. Dasappa, et al., Operational experience on a grid connected 100 kWe biomass gasification power plant in Karnataka, India, Energy sustain. Dev. 15 (3) (2011) 231–239.
[36] S. Tsiakmakis, et al., Experimental study of combustion in a spark ignition engine operating with producer gas from various biomass feedstocks, Fuel (Guildf.) 122 (2014) 126–139.
[37] A.M. Shivapuji, S. Dasappa, In-cylinder investigations and analysis of a SI gas engine fuelled with H2 and CO rich syngas fuel: sensitivity analysis of combustion descriptors for engine diagnostics and control, Int. J. Hydrogen Energy 39 (28) (2014) 15786–15802.
[38] P. Raman, N. Ram, Performance analysis of an internal combustion engine operated on producer gas, in comparison with the performance of the natural gas and diesel engines, Energy (Calg.) 63 (2013) 317–333.
[39] N. Homdoung, N. Tippayawong, N. Dussadee, Effect of ignition timing advance on performance of a small producer gas engine, Int. J. Appl. Eng. Res. 9 (13) (2014) 2341–2348.
[40] P.K. Sharma, et al., An investigation on emissions analysis of spark plug engine fueled by producer gas generated by L. camera, Mater. Today Proc. 46 (2021) 11239–11242.
[41] A. Shah, et al., Performance and emissions of a spark-ignited engine driven generator on biomass based syngas, Bioresour. Technol. 101 (12) (2010) 4656–4661.
[42] N. Indrawan, et al., Engine power generation and emission performance of syngas generated from low-density biomass, Energy Convers. Manag. 148 (2017) 593–603.
[43] S. Szwaja, et al., Sewage sludge producer gas enriched with methane as a fuel to a spark ignited engine, Fuel Process. Technol. 110 (2013) 160–166.
[44] A.K. Thangaiyan, M.M. Mohamed Ibrahim, Production of producer gas and its use as the supplementary fuel for SI engine, Biomass Conver. Biorefin. 13 (6) (2023) 4741–4749.
[45] H. Bundele, et al., Experimental and computational study on the enhancement of engine characteristics by hydrogen enrichment in a biogas fuelled spark ignition engine, Int. J. Hydrogen Energy 47 (71) (2022) 30671–30686.
[46] L.K. Prajapati, J.V. Tirkey, *Performance improvement with boosted intake pressure and hydrogen enriched biogas and producer gas-fuelled SI engine*, Fuel 384 (2025) 133959.
[47] E. Porpatham, A. Ramesh, B. Nagalingam, Effect of swirl on the performance and combustion of a biogas fuelled spark ignition engine, Energy Convers. Manag. 76 (2013) 463–471.
[48] M.J.B. Kabeyi, O.A. Olanrewaju, Technologies for biogas to electricity conversion, Energy Rep. 8 (2022) 774–786.
[49] S.G. Kumar, A. Ramesh, Twin injector biogas diesel RCCI mode-an effective means to reduce NOx emissions without penalty in fuel consumption, Fuel (Guildf.) 352 (2023) 129103.
[50] B. Van Ga, T. Van Nam, T.T.H. Tung, A simulation of effects of compression ratios on the combustion in engines fueled with biogas with variable CO2 Concentrations, J. Eng. Res. Applica. 3 (5) (2013) 516–523. www.ijera.com.
[51] S.K. Hotta, N. Sahoo, K. Mohanty, Comparative assessment of a spark ignition engine fueled with gasoline and raw biogas, Renew. Energy 134 (2019) 1307–1319.
[52] E. Porpatham, A. Ramesh, B. Nagalingam, Effect of compression ratio on the performance and combustion of a biogas fuelled spark ignition engine, Fuel (Guildf.) 95 (2012) 247–256.
[53] S.K. Gupta, M. Mittal, Assessing the influence of compression ratio on engine characteristics including operational limits of a biogas-fueled spark-ignition engine, J. Eng. Gas Turbines Power 142 (12) (2020) 121008.
[54] B. Zhang, et al., Effect of compression ratio and Miller cycle on performance of methanol engine under medium and low loads, Fuel (Guildf.) 351 (2023) 128985.
[55] J. Zhao, Research and application of over-expansion cycle (Atkinson and Miller) engines–A review, Appl. Energy 185 (2017) 300–319.
[56] A. Solouk, et al., Fuel consumption assessment of an electrified powertrain with a multi-mode high-efficiency engine in various levels of hybridization, Energy Convers. Manag. 155 (2018) 100–115.
[57] J. Zhao, et al., Fuel economy improvement of a turbocharged gasoline SI engine through combining cooled EGR and high compression ratio, Energy (Calg.) 239 (2022) 122353.
[58] K. Xing, et al., Thermodynamic analysis of improving fuel consumption of natural gas engine by combining Miller cycle with high geometric compression ratio, Energy Convers. Manag. 254 (2022) 115219.
[59] D. Jia, et al., The effect of variable enhanced Miller cycle combined with EGR strategy on the cycle-by-cycle variations and performance of high compression ratio engines based on asynchronous valve opening strategy, Energy (Calg.) 320 (2025) 135307.
[60] D. Jia, et al., Experiment and simulation analysis of the effects of different asynchronous variable intake valve phase differences on the in-cylinder flow, combustion and performance characteristics of high compression ratio turbocharged enhanced Miller cycle engine, Energy (Calg.) 320 (2025) 134988.
[61] D. Vera, et al., Experimental and economic study of a gasification plant fuelled with olive industry wastes, Energy Sustain. Dev. 23 (2014) 247–257.
[62] A.M. Shivapuji, S. Dasappa, Experiments and zero D modeling studies using specific Wiebe coefficients for producer gas as fuel in spark-ignited engines, Proc. IME C J. Mech. Eng. Sci. 227 (3) (2013) 504–519.
[63] T. Boushaki, et al., Characteristics of biogas and syngas combustion, in: 2019 7th International Renewable and Sustainable Energy Conference (IRSEC), IEEE, 2019.
[64] W.-Q. Wang, Z.-Y. Sun, Experimental studies on explosive limits and minimum ignition energy of syngas: a comparative review, Int. J. Hydrogen Energy 44 (11) (2019) 5640–5649.
[65] J. Huang, R. Crookes, Assessment of simulated biogas as a fuel for the spark ignition engine, Fuel (Guildf.) 77 (15) (1998) 1793–1801.
[66] D. Suresh, E. Porpatham, Influence of high compression ratio and hydrogen addition on the performance and emissions of a lean burn spark ignition engine fueled by ethanol-gasoline, Int. J. Hydrogen Energy 48 (38) (2023) 14433–14448.
[67] R. Chandra, et al., Performance evaluation of a constant speed IC engine on CNG, methane enriched biogas and biogas, Appl. Energy 88 (11) (2011) 3969–3977.
[68] N.P. Bs, K. Gn, Influence of ignition timing on performance and emission characteristics of an SI engine fueled with equi-volume blend of methanol and gasoline, Energy Sources, Part A Recovery, Util. Environ. Eff. 45 (2) (2023) 4652–4666.
[69] S. Yousufuddin, M. Masood, Effect of ignition timing and compression ratio on the performance of a hydrogen–ethanol fuelled engine, Int. J. Hydrogen Energy 34 (16) (2009) 6945–6950.
[70] C. Kurien, P.S. Varma, M. Mittal, Effect of ammonia energy fractions on combustion stability and engine characteristics of gaseous (ammonia/methane) fuelled spark ignition engine, Int. J. Hydrogen Energy 48 (4) (2023) 1391–1400.
[71] S. Tavakoli, et al., Miller cycle application to improve lean burn gas engine performance, Energy (Calg.) 109 (2016) 190–200.
[72] J. Wang, et al., Effects of the continuous variable valve lift system and Miller cycle strategy on the performance behavior of the lean-burn natural gas spark ignition engine, Fuel (Guildf.) 297 (2021) 120762.
[73] H. Park, et al., Comparative assessment of stoichiometric and lean combustion modes in boosted spark-ignition engine fueled with syngas, Energy Convers. Manag. 239 (2021) 114224.
[74] H. Gürbüz, İ.H. Akçay, Evaluating the effects of boosting intake-air pressure on the performance and environmental-economic indicators in a hydrogen-fueled SI engine, Int. J. Hydrogen Energy 46 (56) (2021) 28801–28810.
[75] X. Kan, et al., An investigation on utilization of biogas and syngas produced from biomass waste in premixed spark ignition engine, Appl. Energy 212 (2018) 210–222.
[76] S. Uslu, Optimization of diesel engine operating parameters fueled with palm oil-diesel blend: comparative evaluation between response surface methodology (RSM) and artificial neural network (ANN), Fuel (Guildf.) 276 (2020) 117990.
[77] J.H. Horlock, D. Winterbone, The Thermodynamics and Gas Dynamics of Internal-Combustion Engines, II, 1986.
[78] W.J.D. Annand, Heat transfer in the cylinders of reciprocating internal combustion engines, Proc. Inst. Mech. Eng. 177 (1) (1963) 973–996.

[79] S. Verhelst, C. Sheppard, Multi-zone thermodynamic modelling of spark-ignition engine combustion–an overview, Energy Convers. Manag. 50 (5) (2009) 1326–1335.
[80] D. Mehrnoosh, H.A. Asghar, M.A. Asghar, Thermodynamic model for prediction of performance and emission characteristics of SI engine fuelled by gasoline and natural gas with experimental verification, J. Mech. Sci. Technol. 26 (7) (2012) 2213–2225.
[81] P. Curto-Risso, A. Medina, A.C. Hernández, Optimizing the geometrical parameters of a spark ignition engine: simulation and theoretical tools, Appl. Therm. Eng. 31 (5) (2011) 803–810.
[82] F. Ma, et al., Development and validation of a quasi-dimensional combustion model for SI engines fuelled by HCNG with variable hydrogen fractions, Int. J. Hydrogen Energy 33 (18) (2008) 4863–4875.
[83] F.V. Tinaut, et al., Method for predicting the performance of an internal combustion engine fuelled by producer gas and other low heating value gases, Fuel Process. Technol. 87 (2) (2006) 135–142.
[84] N. Hinton, R. Stone, Laminar burning velocity measurements of methane and carbon dioxide mixtures (biogas) over wide ranging temperatures and pressures, Fuel (Guildf.) 116 (2014) 743–750.
[85] H. John, Internal Combustion Engine Fundamentals, McGraw-Hill Science, 1988.
[86] S.R. Turns, An Introduction to Combustion, 499, McGraw-hill, New York, 1996.
[87] M. Klell, H. Eichlseder, M. Sartory, Mixtures of hydrogen and methane in the internal combustion engine–Synergies, potential and regulations, Int. J. Hydrogen Energy 37 (15) (2012) 11531–11540.
[88] A. Susastriawan, H. Saptoadi, Comparison of the gasification performance in the downdraft fixed-bed gasifier fed by different feedstocks: rice husk, sawdust, and their mixture, Sustain. Energy Technol. Assessments 34 (2019) 27–34.
[89] C. Caligiuri, M. Renzi, Combustion modelling of a dual fuel diesel–producer gas compression ignition engine, Energy Proc. 142 (2017) 1395–1400.
[90] F.M. Group Thermodynamics, W. Annand, Heat transfer in the cylinders of reciprocating internal combustion engines, Proc. Inst. Mech. Eng. 177 (1) (1963) 973–996.
[91] V.G. Bui, et al., Flexible syngas-biogas-hydrogen fueling spark-ignition engine behaviors with optimized fuel compositions and control parameters, Int. J. Hydrogen Energy 48 (18) (2023) 6722–6737.
[92] S. Simsek, S. Uslu, Investigation of the effects of biodiesel/2-ethylhexyl nitrate (EHN) fuel blends on diesel engine performance and emissions by response surface methodology (RSM), Fuel (Guildf.) 275 (2020) 118005.
[93] S.K. Behera, et al., Application of response surface methodology (RSM) for optimization of leaching parameters for ash reduction from low-grade coal, Int. J. Min. Sci. Technol. 28 (4) (2018) 621–629.
[94] S.A. Zaman, D. Roy, S. Ghosh, Process modeling and optimization for biomass steam-gasification employing response surface methodology, Biomass Bioenergy 143 (2020) 105847.
[95] M. Rith, J.B.M.M. Biona, Development of mathematical models for engine performance and emissions of the producer gas-diesel dual fuel mode using Response Surface Methodology, Eng. Appli. Sci. Res. 48 (1) (2021) 18–32.
[96] A. Singh, et al., Optimization of performance and emission characteristics of CI engine fueled with Jatropha biodiesel produced using a heterogeneous catalyst (CaO), Fuel (Guildf.) 280 (2020) 118611.
[97] X. Sun, et al., Numerical investigation of two-stroke marine diesel engine emissions using exhaust gas recirculation at different injection time, Ocean Eng. 144 (2017) 90–97.
[98] R. Wang, et al., Effects of asynchronous late intake valve closing combined with high geometric compression ratio and exhaust gas recirculation on combustion and fuel consumption in a turbocharged SI engine: an experimental study, Energy (Calg.) 290 (2024) 130058.
[99] J. Fu, et al., A comparative study on various turbocharging approaches based on IC engine exhaust gas energy recovery, Appl. Energy 113 (2014) 248–257.
[100] P. Jena, R. Raj, J.V. Tirkey, Thermodynamic performance study and RSM based optimization of SI engine using sewage sludge producer gas blend with methane, Energy (Calg.) 273 (2023) 127179.
[101] L.K. Prajapati, et al., Parametric performance evaluation of SI engine using producer gas-biogas-hydrogen blend as a fuel: a thermodynamic modeling and optimization approach, Int. J. Hydrogen Energy 72 (2024) 268–287.
[102] J. Zareei, A. Kakaee, Study and the effects of ignition timing on gasoline engine performance and emissions, European Transp. Res. Rev. 5 (2013) 109–116.
[103] H. Duan, et al., Regression prediction of hydrogen enriched compressed natural gas (HCNG) engine performance based on improved particle swarm optimization back propagation neural network method (IMPSO-BPNN), Fuel (Guildf.) 331 (2023) 125872.
[104] X. Duan, et al., Experimental and numerical investigation of the effects of low-pressure, high-pressure and internal EGR configurations on the performance, combustion and emission characteristics in a hydrogen-enriched heavy-duty lean-burn natural gas SI engine, Energy Convers. Manag. 195 (2019) 1319–1333.
[105] E. Garcia, et al., Impact of miller cycle strategies on combustion characteristics, emissions and efficiency in heavy-duty diesel engines, SAE Technical Paper 0148-7191 (2020).
[106] M. Gumus, Effects of volumetric efficiency on the performance and emissions characteristics of a dual fueled (gasoline and LPG) spark ignition engine, Fuel Process. Technol. 92 (10) (2011) 1862–1867.
[107] J.V. Tirkey, D.K. Singh, Thermodynamic performance and emission prediction of CI engine fueled with diesel and Vachellia nilotica (Babul) biomass-based producer gas and optimization using RSM, Petrol. Sci. Technol. 40 (9) (2022) 1084–1108.
[108] P. Jena, J.V. Tirkey, Efficiency improvement investigation through Miller cycle strategy for SI engine operating on stoichiometric producer gas and methane blends, Therm. Sci. Eng. Prog. 47 (2024) 102309.
[109] I. Kalargaris, G. Tian, S. Gu, Combustion, performance and emission analysis of a DI diesel engine using plastic pyrolysis oil, Fuel Process. Technol. 157 (2017) 108–115.
[110] Y. Li, et al., Quantitative investigation of the effects of CR, EGR and spark timing strategies on performance, combustion and NOx emissions characteristics of a heavy-duty natural gas engine fueled with 99% methane content, Fuel (Guildf.) 255 (2019) 115803.
[111] L. Siwale, et al., Performance, combustion and emission characteristics of n-butanol additive in methanol–gasoline blend fired in a naturally-aspirated spark ignition engine, Fuel Process. Technol. 118 (2014) 318–326.
[112] V.G. Bui, et al., A simulation study on a port-injection SI engine fueled with hydroxy-enriched biogas, Energy Sources, Part A Recovery, Util. Environ. Eff. 46 (1) (2024) 13706–13722.
[113] V.G. Bui, et al., Enhancing the performance of syngas-diesel dual-fuel engines by optimizing injection regimes: from comparative analysis to control strategy proposal, Process Saf. Environ. Prot. 186 (2024) 1034–1052.
[114] L.L.F. Squaiella, C.A. Martins, P.T. Lacava, Strategies for emission control in diesel engine to meet Euro VI, Fuel (Guildf.) 104 (2013) 183–193.
[115] J.B. Heywood, Internal Combustion Engine Fundamentals, McGraw-Hill Education, 2018.
[116] P. Mojaver, S. Khalilarya, A. Chitsaz, Multi-objective optimization using response surface methodology and exergy analysis of a novel integrated biomass gasification, solid oxide fuel cell and high-temperature sodium heat pipe system, Appl. Therm. Eng. 156 (2019) 627–639.
[117] D. Roy, S. Samanta, S. Ghosh, Performance optimization through response surface methodology of an integrated biomass gasification based combined heat and power plant employing solid oxide fuel cell and externally fired gas turbine, Energy Convers. Manag. 222 (2020) 113182.
[118] M. Singh, S.S. Sandhu, Effect of boost pressure on combustion, performance and emission characteristics of a multicylinder CRDI engine fueled with argemone biodiesel/diesel blends, Fuel (Guildf.) 300 (2021) 121001.
[119] M. Canakci, An experimental study for the effects of boost pressure on the performance and exhaust emissions of a DI-HCCI gasoline engine, Fuel (Guildf.) 87 (8–9) (2008) 1503–1514.
[120] T. Grigoratos, et al., Real world emissions performance of heavy-duty Euro VI diesel vehicles, Atmos. Environ. 201 (2019) 348–359.
[121] S.K. Hotta, N. Sahoo, K. Mohanty, Ignition advancement study for optimized characteristics of a raw biogas operated spark ignition engine, Int. J. Green Energy 16 (1) (2019) 101–113.